/53

Relativistic and Ultrarelativistic Heavy-Ion Collisions. Theoretical Aspects (*)

Joseph Cugnon

University of Liège, Institute of Physics B.5, Sart Tilman, 4000 Liège 1, Belgium

Abstract. — After having identified three energy domains with their characteristic dynamics, the following items are reviewed for each of these domains: the present theoretical knowledge of the relevant static properties of dense matter, the actual status of transport theories, the study of possible direct signals from dense matter and some open problems.

1. Introduction

The principal goal of the heavy-ion collisions is to study nuclear matter under extreme conditions. Very often, the latter is characterized by its static properties. The difficulty of this kind of physics then appears clearly. As the observations involve reaction products, the information on these static properties can be uncovered only through a method which is able to "reconstruct" the collisions. As many degrees of freedom are at work (if one really wants to obtain information on nuclear matter, *i.e.* on an extended system), one cannot rely on simple models. The adequate tools are named "transport theories", which are expected to incorporate static properties, weak gradient transport properties and shorter range phenomena. It is by no means clear that we have a good control on all of these features. It is even less clear that the observables are sensitive to static properties or are determined in a complicated manner by the off-equilibrium features at short scales. Moreover, we do not know whether quantum effects are important or whether they are masked because many degrees of freedom are active. Finally, it is not sure that the numerical methods at our disposal to solve transport equations are accurate.

The "fundamental" theory of nuclear forces is presumably QCD, which involves interactions between quarks and gluons. But a characteristic feature of strong interactions is that they reveal different degrees of freedom when the characteristic energy of the phenomena is changed. Of course, in principle, the true degrees of freedom are those of quark and gluons. But we are forced to use effective degrees of freedom, not only for convenience in the description of the mechanisms, but because calculations in terms of explicit quark and gluon degrees of freedom are

---

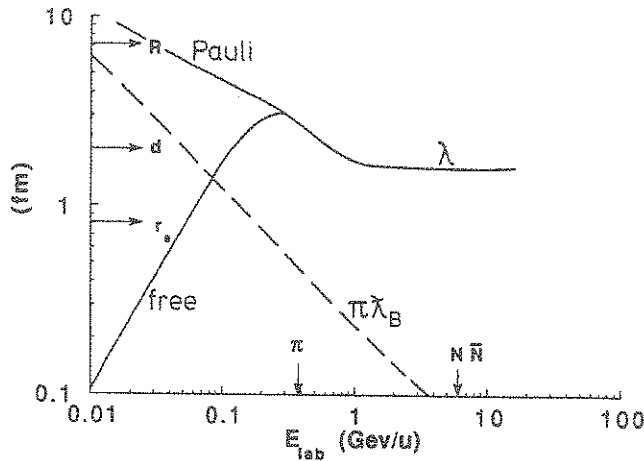(*) Cours donnés à l'école Joliot-Curie en 1995 : Noyaux en collision

Fig. 1. — Comparison between various characteristic lengths: λ = mean free path (free and Pauli blocked), $\lambda_B/2\pi$ = incident nucleon de Broglie wavelength, R = nuclear radius, d = mean internucleon distance, r_s = range of strong nucleon-nucleon force. The arrows indicate the π and $N\bar{N}$ thresholds. See text for details.

only possible for a well-defined class of phenomena (the large Q^2 ones), which apparently has only a very limited importance in heavy-ion collisions. For this reason, the energy range covered by the present review (from ~ 200 MeV/u up to 200 GeV/u) displays a huge variety of concepts, developments and theoretical models. It is not conceivable to cover all of them here. For this reason, a deliberate attitude has been adopted in this review. In each of three energy domains (≤ 1 GeV/u, 1–10 GeV/u, ~ 100 GeV/u), we have attempted to identify the relevant degrees of freedom. Once this is done, we make a short review of the theoretical knowledge of infinite nuclear matter in the selected regime, of the status of the transport theory, on the essential theoretical results and on the possible signals of the temporarily dense matter. We have deliberately, because of lack of space, left behind detailed comparison with experiment and the elaboration of the theories, limiting ourselves to a as clear as possible presentation of the basic concepts and, sometimes, of the open theoretical problems.

2. Identification of the Relevant Degrees of Freedom

Table I below gives a qualitative idea of the relevant degrees of freedom and some characteristic quantities which allow to grossly determine the corresponding dynamics and crudely delineate the boundaries of the energy domain where they are prevailing. In the relatively small energy domain, the method allowing to identify the dynamics is illustrated in Figure 1. Here, the de Broglie wavelength of an incident nucleon is shown and compared to characteristic lengths. One immediately sees that above $E_{lab} \sim 0.1$ GeV/u, this wavelength is smaller than the average

Table I.

	Mean Field	Nucleon Cascades	Hadronic Cascades	Partonic Cascades
E_{lab}	≤ 20 MeV/u	0.02–2 Gev/u	2–10 GeV/u	10–200 GeV/u
Dynamics	mean field	NN collisions	NN collisions + hadron prod.	string dynamics
Typical length	a few fm	1 fm	0.5 fm	0.1 fm
Typical energy	$\hbar\omega_{osc}$	100 MeV	a few hundreds MeV	?
Typical time	a few fm/c	~1 fm/c	< 1 fm/c	?
Structure	nucleon wave function	(point) nucleon	nucleon & resonances	partons & strings
Input	V_{eff}	σ_{eff}	σ_{el} & σ_{inel}	string formation and fragmentation probabilities
Energy loss	Fermi dynamics	collisions	particles production	string formation
Models	TDHF FMD	BUU INC VUU LV BL KB QMD FMDC	INC ARC QMD	VENUS DPM FRITIOF
Equation of state	←——— Fermi liquid equation of state ———→ <hadronic fluid>			string fluid

distance between neighbouring nucleons in the target and smaller than the mean free path. Therefore, it is expected that the relevant degrees of freedom are those of the nucleons and that the dynamics is dominated by binary interactions. In the same Figure, the threshold for meson production is indicated as well as the one for the creation of a nucleon-antinucleon pair. One can then realize that one is shifting progressively from a regime where the degrees of freedom are those associated with the translation of the nucleons to a regime where the fundamental objects are hadrons and where the relevant degrees of freedom are including more and more mesonic degrees of freedom.

Going up in energy, one expects the internal degrees of freedom of hadrons to show up progressively. The situation is more complicated here as the properties of the substructures of the hadrons are changing with the scale of the four-momentum transfer Q under which they are probed. If this scale is very large, as in lepton deep inelastic collisions, the substructures are the partons. They can then interact independently of each other, if $Q^2 > \Lambda^2$, $\Lambda \approx 200$ MeV being the renormalization scale of QCD. This condition does not delineate precisely a particular range of incident energy, since, as we will see, the motion is largely longitudinal in the collisions. As a consequence, in a given nucleus-nucleus collision, hard processes at large Q^2 are mixed with soft processes, why imply a "collection of partons" that, in some limit, may be viewed as valence quarks. The situation is more complicated by the fact that these entities carry colour and that colour is confined. We will see that the basic interaction mechanism is then dominated by the formation of "strings". This picture has arisen from the phenomenology of the hadron-hadron scattering at high energy, as revealed in the seventies at the ISR. In short, at the BEVALAC-SIS energies, the relevant degrees of freedom are those of the nucleons. At the AGS energies, they coincide with the hadron degrees of freedom. At ISR and SPS (presumably), they are identified to those of strings, to a large extent. Expectedly, at the LHC, they will be those of the partons, quarks and gluons.

3. BEVALAC-SIS Energies

3.1. Static Properties of Nuclear Matter

3.1.1. Equation of State. — At zero temperature, the experimental knowledge of the equation of state $U/A(\rho)$ reduces to the coordinates of the equilibrium point ($\rho_0 = 0.17$ fm^{-3} and $U/A(\rho_0) = -16$ MeV) and to the compressibility $K = (220 \pm 20)$ MeV. From the theoretical point of view, the situation is far from ideal, as shown in Figure 2. At first sight, there is concordance between lowest order Brueckner calculations [1], Dirac-Hartree-Fock calculations at the same order [2] and the variational calculations of Friedman and Pandharipande [3], that all assume point-like nucleons interacting through potentials. However, it should be stressed that the calculation of Friedman and Pandharipande reproduces the saturation point correctly only at the expense of the introduction of an adjusted purely phenomenological attractive three-body force, that contributes for ~ 5 MeV at $\rho = \rho_0$! Figure 2 also gives an idea of the theoretical uncertainties, once one goes
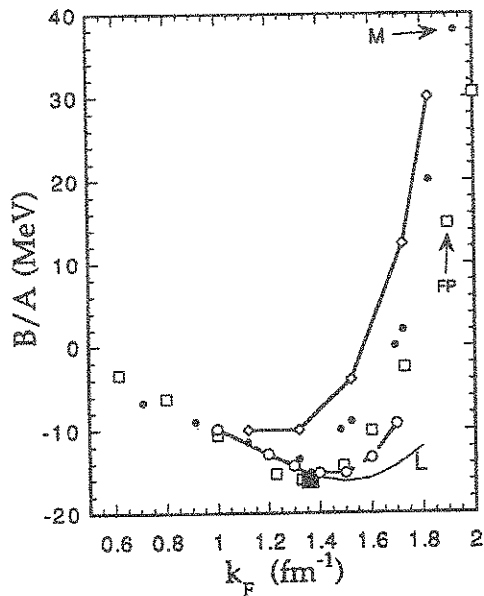
Fig. 2. — Comparison between various calculations of nuclear matter equation of state: Brueckner calculation of reference [1] (thin line), relativistic calculation of reference [2] (black dots), variational calculation of reference [3] (open squares). The losanges give the results of reference [2], when Δ degrees of freedom are included. The open dots correspond to the results of reference [1] when three-body forces are included. The black square gives the experimental saturation point.

beyond the picture of structureless nucleons. The losanges give Malfliet's results [2] when the Δ degrees of freedom are included and the open circles correspond to the calculation of the Liège group [3] when three-body forces are included, a large part of them coming from the graphs with Δ intermediate states. This feature is in keeping with our remark about the progressive change of regime.

3.1.2. Momentum Distribution and Single-Particle Strength. — The momentum distribution is defined by

$$n\,(k) = \langle 0|a_k^\dagger a_k|0\rangle, \tag{3.1}$$

where $|0\rangle$ is the ground state and $a_k^\dagger$, a_k are the usual creation and annihilation operators. It can be related to the ordinary (causal) Green function

$$G\,(k,\omega) = \int dt e^{i\omega t}\,(-i)\,\langle 0|T\left[a_k\,(t)\,a_k^\dagger\,(0)\right]|\rangle \tag{3.2}$$

which has the following representation

$$G\,(k,\omega) = \int_{-\infty}^{+\infty} dE\frac{S\,(k,E)}{\omega - E} \tag{3.3}$$

with

$$
\begin{aligned}
S\left(k,E\right) &= \int \mathrm{d}E' \left(\left| \langle \phi_{E'}^{\dagger} | a_k^{\dagger} | 0 \rangle \right|^2 + \left| \langle \phi_{E'}^{-} | a_k | 0 \rangle \right|^2 \right) \delta\left(E - E'\right) \\
&= S_p\left(k,E\right) + S_h\left(k,E\right)
\end{aligned}
\tag{3.4}
$$

$S_h\left(k,E\right)$, that we call also $a\left(k,E\right)$ below, measures the probability to go to a state at $\left(A-1\right)$ particles of energy E when removing a particle with momentum k. One has [4]

$$
\int_{-\infty}^{\mu} S_h\left(k,E\right) \mathrm{d}E = n\left(\mathrm{k}\right),
\tag{3.5}
$$

where μ is the chemical potential. For independent particles

$$
S_h\left(k,E\right) = \delta\left(E - e\left(k\right)\right) \quad , \quad n\left(\mathrm{k}\right) = 1 \quad , \quad k < k_{\mathrm{F}},
\tag{3.6}
$$

where $e\left(k\right)$ is the single-particle energy. In nuclear matter and in actual nuclei, the situation is close to (3.6), but there are departures from this ideal case: the momentum density lies around 0.7–0.8 (see [5] for nuclear matter, and [6] for a compilation for nuclei) and the single particle strength S_h is close to a delta function in the vicinity of the Fermi surface only [7].

3.1.3. Excitations of Nuclear Matter. — The single particle excitations are the best documented. Theoretically, they correspond to the pole of the Green function (3.2), which in all generality, may be written as

$$
G\left(k,\omega\right) = \cfrac{1}{\omega - \frac{k^2}{2m} - M\left(k,\omega\right)},
\tag{3.7}
$$

where $M\left(k,\omega\right)$ is the so-called mass operator or self-energy, which may be complex. For nuclear matter (as for nuclei), there is generally only one pole for a given $\mathbf{k}$, confirming the validity of the quasi-particle concept, whose energy $e\left(k\right)$ is given by the equation

$$
e\left(k\right) = \frac{k^2}{2m} + M\left(k, e\left(k\right)\right).
\tag{3.8}
$$

The (real part) of the second term may be viewed as the potential $U\left(k\right)$ felt by the nucleons. For energies ranging from ~ 10 to ~ 80 MeV above the Fermi level, one has, in good approximation [8]

$$
e\left(k\right) = e\left(0\right) + \frac{\hbar^2 k^2}{2m^*},
\tag{3.9}
$$

with $m^*/m \approx 0.7$. At higher energy and higher temperature, it seems that $m^* \to m$ whatever k is [9].

The collective excitations of nuclear matter are not well-known. They are often studied within the Landau theory for Fermi liquids. The latter predicts the existence of zero sound, which may correspond in actual nuclei to the quadrupole resonance.

3.2. Transport Theory

3.2.1. Theoretical Framework. — The derivation of a transport equation may be done in several ways. For reasons which will appear more clearly later on, we adopt here the method of real time Green functions, used for the first time by Kadanoff and Baym [10]. This formalism has been improved later by Danielewicz [11] and by Malfliet [12]. We will closely follow this reference. Starting from the Hamiltonian for fermions

$$H = \int d^3x \psi^+(x,t) \left(-\frac{\hbar^2}{2m}\Delta\right) \psi(x,t) \tag{3.10}$$
$$+ \int d^3x_1 \int d^3x_2 \int d^3x_3$$
$$\times \int d^3x_4 \langle x_1 x_2 | V | x_3 x_4 \rangle \psi^+(x_1,t)\psi^+(x_2,t)\psi(x_4,t)\psi(x_3,t)$$

where the fermion field operators follow the usual anticommutation relations, one may define several Green functions

$$g(1,1') = -i\langle T\psi(1)\psi^+(1')\rangle \quad , \quad g^a(1,1') = -i\langle T^a\psi(1)\psi^+(1')\rangle$$
$$g^>(1,1') = -i\langle \psi(1)\psi^+(1')\rangle \quad , \quad g^<(1,1') = i\langle \psi^+(1')\psi^+(1)\rangle \tag{3.11}$$

where T^a is the antichronological operator and where $1 = (\mathbf{r},t)$, $1' = (\mathbf{r}',t')$. These Green functions are not independent. One has

$$g(1,1') = g^>(1,1')\theta(t-t') + g^<(1,1')\theta(t'-t)$$
$$g^a(1,1') = g^>(1,1')\theta(t'-t) + g^<(1,1')\theta(t-t'). \tag{3.12}$$

We will consider $g^>$ and $g^<$ below. $g(1,1')$ is the same Green function as (3.7). Finally, $g^<$ is of crucial importance: at equal times, it reduces to the density operator of the system

$$\lim_{t' \to t} g^<(1,1') = -i\rho(\mathbf{r},\mathbf{r}',t). \tag{3.13}$$

The starting point of the derivation of the transport equation is the Dyson equations fulfilled by these Green functions

$$\left(-i\partial_{t_1} + \frac{\hbar^2\Delta_1}{2m}\right) g^{\lessgtr}(1,1') =$$
$$\int_{-\infty}^{+\infty} d1'' \left[\sum^+(1,1'')\, g^{\lessgtr}(1'',1') + \sum^{\lessgtr}(1,1'')\, g^-(1'',1') \right] \tag{3.14}$$
$$\left(-i\partial_{t_1'} + \frac{\hbar^2\Delta'_1}{2m}\right) g^{\lessgtr}(1,1') =$$
$$\int_{-\infty}^{+\infty} d1'' \left[g^+(1,1'')\, \sum^{\lessgtr}(1'',1') + g^{\lessgtr}(1,1'')\, \sum^-(1'',1') \right]$$

where, in order to simplify the notation, we have introduced $F^{\pm} = \pm\theta(\pm(t-t'))$ $[F^{>} - F^{<}]$, with $F = \Sigma$ or g. The mass operators $\sum^{>}_{<}$ can be viewed as the sum of all irreducible diagrams corresponding to the propagation indicated by $g^{>}_{<}$. One then transforms (3.14) by taking the sum and the difference. Further, one introduces the coordinates

$$t = \frac{1}{2}(t+t') \ , \ \mathbf{r} = \frac{1}{2}(\mathbf{r}+\mathbf{r}') \ , \ \tau = t - t' \ , \ \rho = \mathbf{r} - \mathbf{r}', \qquad (3.15)$$

where we have reused $\mathbf{r}$ and t as the average coordinates, in order to avoid proliferation of symbols, and the Wigner transforms ($h = \Sigma$ or g)

$$h(p,x) = \int \mathrm{d}^4 x e^{\frac{i}{\hbar}px} h\left(\mathbf{r} + \frac{\rho}{2} \ , \ t + \frac{\tau}{2} \ , \ \mathbf{r} - \frac{\rho}{2} \ , \ t - \frac{\tau}{2}\right) \qquad (3.16)$$

where $p = (\mathbf{p}, \omega)$, $x = (\mathbf{r}, t)$. This enables to expand non local quantities around the space time point $(\mathbf{r}, t)$.

It is usual to introduce, at this point, the weak gradient approximation, consisting in developing $h(p,x)$ in Taylor expansions limited to the first order terms. One so obtains

$$\left(\partial_t + \frac{\mathbf{p}}{m} \cdot \nabla\right) g^{>}_{<}(p,x) - i\left\{\mathrm{Re}\Sigma^+(p,x), g^{>}_{<}(p,x)\right\} -$$
$$i\left\{\Sigma^{>}_{<}(p,x), \mathrm{Re}\, g^+(p,x)\right\} = \Sigma^{>}(p,x)g^{<}(p,x) - \Sigma^{<}(p,x)g^{>}(p,x), \qquad (3.17)$$

where the (four-dimensional) Poisson bracket is defined by

$$\{A,B\} = \partial_p A.\partial_x B - \partial_x A.\partial_p B. \qquad (3.18)$$

The equations (3.17) are absolutely general (except for the weak gradient approximation) and are known as the Kadanoff-Baym equations. They have the general structure of the transport equations, with a drift term on the l.h.s. and a collision term on the r.h.s..

One can see that equations (3.17) generalize the ordinary classical transport (Boltzmann-like) equations. Let us write

$$g^{<}(p,x) = ia(p,x)F(p,x) \ , \ g^{>}(p,x) = -ia(p,x)[1 - F(p,x)]. \qquad (3.19)$$

Using equation (3.12) and the properties of Fourier transforms, one sees that (if $F \to \theta(\mu - e(p))$ at equilibrium, see below), $a(p,x)$ reduces to $S(\mathbf{k},\omega)$, defined in equation (3.3). Thus, $a(p,x)$ can be viewed as the dynamical spectral function. An equation for the latter quantity can be obtained by considering the difference between the two equations (3.17). One gets, using (3.18)

$$\left\{\omega - \frac{p^2}{2m} - \mathrm{Re}\,\Sigma^+(\omega), a(\omega)\right\} - i\left\{\Sigma^{>}(\omega) - \Sigma^{<}(\omega), \mathrm{Re}\, g^+(\omega)\right\} = 0, \quad (3.20)$$

where we have explicitated the ω-dependence only. Owing to the definition of $F^{\pm}$, equation (3.20) can easily be transformed as

$$\left\{\omega - \frac{p^2}{2m} - \mathrm{Re}\,\Sigma^+(\omega) - i\,\mathrm{Im}\,\Sigma^+(\omega), a(\omega)\right\} = 0, \qquad (3.21)$$

which means that

$$a = f\left(\omega - \frac{p^2}{2m} - \operatorname{Re}\sigma^+(\omega) - i\operatorname{Im}\Sigma^+(\omega)\right),\qquad(3.22)$$

where f is an arbitrary function. It has to be determined from the initial conditions, whose form may be found in [4], for instance:

$$a(p,x) = \frac{-2\operatorname{Im}\Sigma^+}{\left(\omega - \frac{p^2}{2m} - \operatorname{Re}\Sigma^+\right)^2 + (\operatorname{Im}\Sigma^+)^2}.\qquad(3.23)$$

It remains to derive an equation for $F(p,x)$. Summing the equations (3.17), one arrives at

$$\left\{\omega - \frac{p^2}{2m} - \operatorname{Re}\Sigma^+, F\right\} - \frac{1}{a}\left\{\Sigma^> + \Sigma^<, P\int\frac{a(p,\omega')}{\omega-\omega'}d\omega'\right\} = \Sigma^> F - \Sigma^<(1-F).\qquad(3.24)$$

In the limit where $\operatorname{Im}\Sigma^+ = \Sigma^> - \Sigma^< \to 0$,

$$a(p,x) \to \delta(\omega - e(p,x)) = \frac{p^2}{2m} + \operatorname{Re}\Sigma^+(p,x),\qquad(3.25)$$

a Boltzmann-like equation is recovered for the quantity

$$f = f(\mathbf{p},x) = f(\mathbf{p},\mathbf{r},t) = F(\mathbf{p}, e(\mathbf{p},x), \mathbf{r}, t).\qquad(3.26)$$

The connection with the Boltzmann equation becomes clearer when the ingredients of (3.17) and (3.24) are given in lowest order in the interaction (and at the classical level, Eq. (3.25))

$$\Sigma^\lessgtr(p,x) = \int\frac{d^3p'}{(2\pi)^3}\int\frac{d^3\bar{p}}{(2\pi)^3}\int\frac{d^3\bar{p}'}{(2\pi)^3}(2\pi)^4\delta(\mathbf{p}+\mathbf{p}'-\bar{\mathbf{p}}-\bar{\mathbf{p}}')\delta(e(p)+e(p')$$

$$-e(\bar{p})-e(\bar{p}'))\,|\langle\mathbf{pp}|V|\bar{\mathbf{p}}\bar{\mathbf{p}}'\rangle|^2\left\{\begin{array}{c}f(p')(1-f(\bar{p}))(1-f(\bar{p}'))\\[2mm](1-f(p'))f(\bar{p})f(\bar{p}')\end{array}\right.,\qquad(3.27)$$

where the $\mathbf{r}, t$-dependences entering (3.26) are not explicitated, and

$$\operatorname{Re}\Sigma^+(p,x) = \int\frac{d^3p'}{(2\pi)^3}\langle pp'|V|pp'\rangle f(p')\qquad(3.28)$$

$$\begin{aligned}\operatorname{Im}\Sigma^+(p,x) = {} & \frac{1}{2}\int\frac{d^3p'}{(2\pi)^3}\int\frac{d^3\bar{p}}{(2\pi)^3}\int\frac{d^3\bar{p}'}{(2\pi)^3}(2\pi)^4\\ & \delta(\mathbf{p}+\mathbf{p}'-\bar{\mathbf{p}}-\bar{\mathbf{p}}')\delta(e(p)+e(p')-e(\bar{p})-e(\bar{p}'))\\ & |\langle\mathbf{pp}'|V|\bar{\mathbf{p}}\bar{\mathbf{p}}'\rangle|^2 f(p')(1-f(\bar{p}))(1-f(\bar{p}')).\qquad(3.29)\end{aligned}$$

For the strong interactions, like nuclear forces, one can sum up all ladder diagrams, corresponding to particles scattering on each other (*i.e.* interacting) many times, before separating and interacting with other particles. This is the T-matrix approximation. If one further considers the interaction of the two particles with the rest of the system as if the latter provides an average field for the scattering particles, one obtains the g-matrix approximation. In equations (3.27–3.29), one then should make the substitution

$$\langle \mathrm{pp}' |V| \overline{\mathrm{p}} \ \overline{\mathrm{p}}' \rangle \rightarrow \langle \mathrm{pp}' |g| \overline{\mathrm{p}} \ \overline{\mathrm{p}}' \rangle \tag{3.30}$$

where g is the solution of the Bethe-Goldstone equation

$$\langle \mathrm{pp}' |g| \overline{\mathrm{pp}}' \rangle = \langle \mathrm{pp}' |V| \overline{\mathrm{p}} \ \overline{\mathrm{p}}' \rangle + \int \frac{\mathrm{d}^3 p_1}{(2\pi)^3} \int \frac{\mathrm{d}^3 p_2}{(2\pi)^3}$$

$$\langle \mathrm{pp}' |V| \mathrm{p}_1 \ \mathrm{p}_2 \rangle \frac{(1 - f(p_1))(1 - f(p_2))}{e(p) + e(p') - e(p_1) - e(p_2)} \langle \mathrm{p}_1 \ \mathrm{p}_2 |g| \overline{\mathrm{p}} \ \overline{\mathrm{p}}' \rangle. \tag{3.31}$$

3.2.2. Quantum Effects. — The latter can be studied by comparing the solutions of (3.24) with those of Boltzmann equation. This could be done on simple cases only. For instance, Malfliet [12] has studied the thermalisation of a fast particle in an infinite medium: one may so neglect the $\Sigma^<$ term in equation (3.24). Neglecting further the effect of Re Σ^+ in the drift term, one obtains, in the classical case, the following equation

$$\frac{\partial}{\partial t} f(\mathrm{p}, t) = -\Lambda f(\mathrm{p}, t) \tag{3.32}$$

for the evolution of the probability distribution representing the incident particle (we will consider $\Lambda = \Sigma^>$ as a constant for simplicity). For the quantum case, one gets, with the help of (3.23) and (3.24)

$$\frac{\partial}{\partial t} f = -\Lambda \left[1 + \left(\frac{\omega - \frac{p^2}{2m} - \mathrm{Re}\ \Sigma^+}{\Lambda} \right)^2 \right] f. \tag{3.33}$$

Integrating over ω for the sake of comparison at a given p, one obtains

$$\frac{\partial f(t)}{\partial t} = -\Lambda_Q f(t), \tag{3.34}$$

with

$$\Lambda_Q = \Lambda \frac{\mathrm{e}^{-x^2}}{\pi x\ \mathrm{Erfc}(x)} \quad , \quad x = \sqrt{\Lambda t}, \tag{3.35}$$

where Erfc (x) is the error function. The ratio between the function $f(t)$ in the classical and quantum cases is given in Figure 3. The relaxation is much slower in the quantum case for large Λ, *i.e.* for high collision rate. This is understandable as, intuitively, quantum effects are expected to increase with the importance of

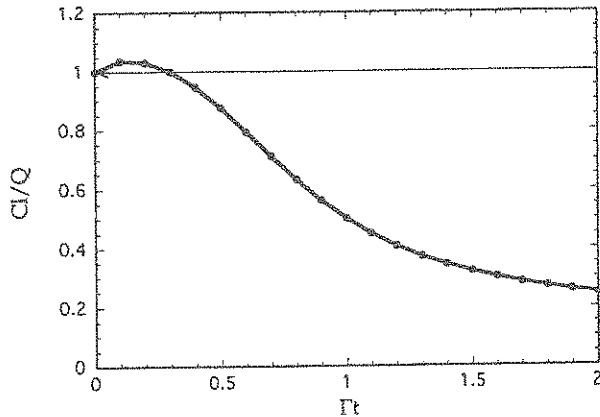Fig. 3. — Ratio between the classical and quantum relaxation rates as a function of the product of the collision rate Γ and time t. Adapted from reference [12].

collisions. We want to stress that the quantum effects we are discussing here are linked with the width of the strength function (3.23), *i.e.* with the fact that the dispersion relation of *interacting* particles is not fixed completely. They are off-energy shell and they recover the energy shell when the collisions cease. The quantum effects linked with the wave nature of the particle motion is not taken into account here as the latter implies higher order terms in the gradient expansion [13].

Let us finally remark that an alternative formulation of the quantum transport equation taking the form of an equation for the quantity $f(\mathbf{r}, \mathbf{p}, \tau, t)$ which is obtained by Wigner transforming the quantity $g^<(1, 1')$ (Eq. (3.12)) on the space coordinates only [10,11] (see Eqs. (3.15) and (3.16)). The equation is non local in time. Köhler has recently solved this equation for the case of two infinite nuclear matters in relative motion [14]. He also notices a slowing down of the equilibration process, compared to the classical case, but not as spectacular as in Figure 3.

3.2.3. Medium Effects. — They influence all the different terms of the transport equations, even at the classical level. They imply the use of the g-matrix in equations (3.27–3.29) instead of the T-matrix in the collision term and in the mean field term, and the introduction of the single-particles energies in the argument of the energy conserving delta function, instead of the kinetic energies. For the collision terms, medium effects can be taken into account by using effective collision cross-sections, as underlined in [15]. Up to now, this has been done by introducing local correction factors depending on the local density and temperature (averaging so on $\mathbf{p}'$ in equation (3.27)). As an illustration, we give in Figure 4 this correction factor for collisions undergone by a nucleon of energy E relative to a surrounding matter at zero temperature, as calculated in [15,16]. One notices at small densities a striking enhancement, precursor of the superfluid phase. In actual heavy-ion collisions, it is not expected to see such an enhancement, which would require some time and
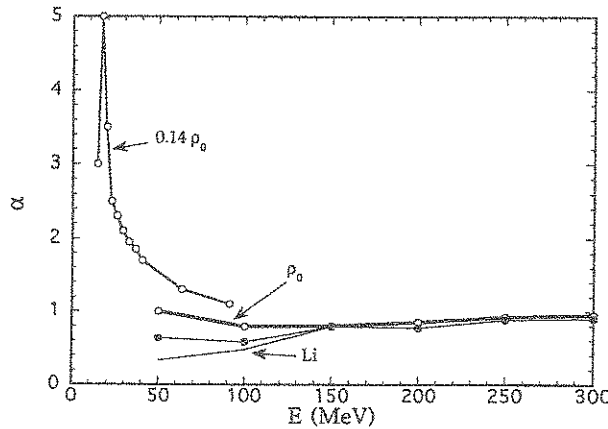
Fig. 4. — Ratio between the effective and free nucleon-nucleon cross-sections, as calculated in reference [15] (two upper curves) and reference [16] (two lower curves, for $\rho = \rho_0/2$ and ρ_0, from top to bottom).

some spatial coherence to develop. Let us also remark that the two calculations do not really agree at small energy.

Owing to (3.18), the l.h.s. of equation (3.24) has a typical drift term form, which at the limit Im $\Sigma^+ \to 0$, writes

$$\left(\frac{\partial}{\partial t} + \frac{\mathbf{p}}{m} \cdot \nabla - (\nabla U) \cdot \nabla_p + (\nabla_p U) \cdot \nabla \right) f = G - L, \qquad (3.36)$$

where the average potential U depends, because of (3.29), on the particle momentum (one rather speaks somewhat incorrectly of a velocity dependence). This generalizes the optical potential, which can be described in the static case as the folding of the g-matrix with the density [4,8]. In this case, U is basically a quadratic function of p and one can advantageously group the second and fourth terms in (3.36) can be advantageously put together by the introduction of an effective mass

$$\frac{1}{m^*} = \frac{1}{m} + \frac{1}{p} \frac{\partial U}{\partial p}, \qquad (3.37)$$

consistent with definition (3.9) in this case. In the dynamical case, it is not sure that the constant effective mass approximation is justified. Furthermore, this effective mass may vary with the properties of the matter. In [9], it is shown that m^* lies close to m for temperatures above 70–80 MeV.

Within the constant effective mass approximation, the delta function for energy conservation writes

$$\delta \left(e\left(p \right) + e\left(p' \right) - e\left(\bar{p} \right) - e\left(\bar{p}' \right) \right) = \frac{m^*}{m} \delta \left(\frac{p^2}{2m} + \frac{p'^2}{2m} - \frac{\bar{p}^2}{2m} - \frac{\bar{p}'^2}{2m} \right). \qquad (3.38)$$

The m^*/m factor is quite often neglected in numerical simulations.

3.2.4. *Numerical Methods.* — There are basically two approaches to the numerical treatment of transport equations: the pseudo-particles method and the simulation method. The first one aims to solve transport equation for the quantity (3.26) by sampling this function with test particles satisfying the following Hamilton equation

$$\dot{\mathbf{r}} = \frac{\mathbf{p}}{m} + \nabla_{\mathbf{p}} \, U\,(\mathbf{r}, \mathbf{p}) \,, \tag{3.39}$$

$$\dot{\mathbf{p}} = -\nabla_r \, U\,(\mathbf{r}, \mathbf{p}) \,, \tag{3.40}$$

where the potential $U\,(\mathbf{r}, \mathbf{p})$ can be written as

$$U\,(\mathbf{r}, \mathbf{p}) = \int V_{\text{eff}}\,(\mathbf{r} - \mathbf{r}', \mathbf{p} - \mathbf{p}')\, f\,(\mathbf{r}', \mathbf{p}', t)\, \mathrm{d}^3 r' \mathrm{d}^3 p' , \tag{3.41}$$

the function $f\,(\mathbf{r}, \mathbf{p}, t)$ being given in turn by

$$f\,(\mathbf{r}, \mathbf{p}, t) = \sum_{i=1}^{N_{\overline{p}}} g\,(\mathbf{r} - \mathbf{r}_i\,(t)\,, \, \mathbf{p} - \mathbf{p}_i\,(t))\,, \tag{3.42}$$

where the sum runs over the quasi-particles. In the last expression, g is a profile function introduced to smoothen the function f and the mean field U. This method can be shown to handle the drift part (l.h.s.) of equation (3.36) correctly (see [17] for an extensive discussion), the collision term being treated as below. The general attitude is to chose the effective interaction freely, provided it reproduces the binding of nuclear matter in the same approximation as the transport equation itself, *i.e.*

$$\frac{B}{A} = \frac{1}{\rho} \int_{|\mathbf{k}| \, < \, k_{\mathrm{F}}} \frac{\mathrm{d}^3 k}{(2\pi)^3} \left(\frac{k^2}{2m} + \frac{1}{2} \, U\,(\mathbf{k}) \right) \tag{3.43}$$

$$= \frac{3}{5} \frac{k_{\mathrm{F}}^2}{2m} + \frac{1}{2} \int_{|\mathbf{k}| \, < \, k_{\mathrm{F}}} \frac{\mathrm{d}^3 k}{(2\pi)^3} \int_{|\mathbf{k}'| \, < \, k_{\mathrm{F}}} \frac{\mathrm{d}^3 k}{(2\pi)^3} \int \mathrm{d}^3 r' \, V_{\text{eff}}\,(\mathbf{r} - \mathbf{r}'\,, \, \mathbf{p} - \mathbf{p}')\,.$$

Several forces have been used, including momentum dependent ones.

In the second approach, one tries to keep the fluctuations at the highest level (in the sense of distribution functions). The idea is that fluctuations arise from collisions. Their very nature has never been very much discussed, but it is supposed to follow from a stochastic description of the nucleon-nucleon final states, with a probability law proportional to relevant differential cross-sections. In some sense, this method preserves quantum fluctuations. The key point is then to assume that the evolution of the A-body density matrix (or the Wigner transforms ([1])) is given by the classical evolution of an ensemble of classical (spike-like) A-body distribution functions

$$f_{\mathrm{W}}^A\,(\mathbf{r}_1, ... \mathbf{r}_A, \mathbf{p}_1, ... \mathbf{p}_A, t) = \int \mathrm{d}\omega \, g\,(\omega) \, f_A\,(\mathbf{r}_1, ... \mathbf{r}_A, \mathbf{p}_1, ... \mathbf{p}_A, \omega, t)\,, \tag{3.44}$$

([1]) We disregard here the problem of the positiveness of the Wigner function.

$$f_A\left(\mathbf{r}_1, ...\mathbf{r}_A, \mathbf{p}_1, ...\mathbf{p}_A, t\right) = \delta\left(\mathbf{r}_1 - \mathbf{r}_1\left(\omega, t\right)\right)...\delta\left(\mathbf{p}_A - \mathbf{p}_A\left(\omega, t\right)\right), \qquad (3.45)$$

$\mathbf{r}_1\left(\omega, t\right), ...\mathbf{p}_A\left(\omega, t\right)$ giving the trajectories of the particles in the realization ω, and where $g\left(\omega\right)$ is the (usually uniform) probability distribution governing the simulation. The linearity (3.44) guarantees the same relationship for all $s < A$ distribution functions. The hypothesis (3.44) is far from having a trivial content. If at the initial time, one can easily admit that it is not too difficult to generate $g\left(\omega\right)$ which satisfies (3.44), *i.e.* to have a good sampling of the initial state, it is by no means guaranteed that the same $g\left(\omega\right)$ is good for any later time. To be more specific, let $U^A\left(x, x', t, t_0, \omega\right)$ be the evolution operator of the function $f_A\left(x, \omega, t\right)$ (provided it exists), where we used the compact notation x for $\mathbf{r}_1, ..., \mathbf{p}_A$. One has

$$f_A\left(x, \omega, t\right) = \int \mathrm{d}x'\ U^A\left(x, x', t, t', \omega\right) f_A\left(x', \omega, t'\right) \qquad (3.46)$$

and

$$\int \mathrm{d}\omega\ g\left(\omega\right) f_A\left(x, \omega, t\right) = \int \mathrm{d}\omega\ g\left(\omega\right) \int \mathrm{d}x'\ U^A\left(x, x', t, t', \omega\right) f_A\left(x', \omega, t'\right). \quad (3.47)$$

The operator U^A may depend much upon ω, but it is conceivable that there exists an operator $U^A_{\mathrm{eff}}\left(x, x', t, t_0\right)$ such that

$$\int \mathrm{d}\omega\ g\left(\omega\right) f_A\left(x, \omega, t\right) \approx \int \mathrm{d}x'\ U^A_{\mathrm{eff}}\left(x, x', t, t_0\right) \int \mathrm{d}\omega\ g\left(\omega\right) f_A\left(x', \omega, t'\right). \quad (3.48)$$

This is not surprising as it happens in many diffusion problems: this corresponds, for instance, to the equivalence of the Langevin equations and the Fokker-Planck equations for Brownian motion. One cannot be sure however that the evolution operator U^A_{eff} is equivalent to the one for the Wigner function f_W^A. This is probably true for the l.h.s. of the transport equation, if the mean field is generated by the average one-body distribution function (as it is the case for the so-called parallel ensemble [18]), but there is no indication for the r.h.s.. If this holds, the second method is by far superior to the first one as it propagates correlations to all order. However, some effects of correlations may be obtained in the first method by the adjunction of fluctuating terms, as we shortly explain below.

3.2.5. Fluctuations. Boltzmann-Langevin Equations. — It is easier here to start from the BBGKY hierarchy than from the Green functions. We will stay at the classical level, since we want to concentrate on classical fluctuations. We will follow closely the notation of [19]. The first equations of the hierarchy write

$$\left(\partial_t - L_1^0\right) f_1\left(x_1, t\right) = \int \mathrm{d}x_2\ L'_{12}\ f_2\left(x_1, x_2, t\right) \qquad (3.49)$$

$$\left(\partial_t - L_1^0 - L_2^0\right) f_2\left(x_1, x_2, t\right) = L'_{12}\ f_2\left(x_1, x_2, t\right) \qquad (3.50)$$
$$+ \int \mathrm{d}x_3 \left(L'_{13} + L'_{23}\right) f_3\left(x_1, x_2, x_3, t\right),$$

where L_i^0 is the free Liouvillian (basically the drift term), L_{ij}' the interaction Liouvillian and where x_i stands for $\mathbf{r}_i, \mathbf{p}_i$. The usual method yielding Boltzmann equation consists in assuming that f_3 factorizes in products of $f_2 f_1$, solving (3.50) for f_2 assuming that at time t_0, f_2 factorizes in a product of two f_1's and inserting the solution in (3.49). One may take account of the correlations by relaxing the last hypothesis, writing

$$f_2(x_1, x_2, t_0) = f_1(x_1, t_0) f_1(x_2, t_0) + \delta f_2(x_1, x_2, t_0).\qquad (3.51)$$

The solution of (3.50) at $t > t_0$ is formally given by

$$f_2(x_1, x_2, t_0) = f_1(x_1, t) f_1(x_2, t) + \int_{t_0}^{t} dt' \; e^{\left(L_1^0 + L_2^0\right)t'} L_{12}' \; f_1(x_1, t') f_1(x_2, t')$$

$$+ e^{\left(L_1^0 + L_2^0\right)(t - t_0)} \delta f_2(x_1, x_2, t_0).$$
$$(3.52)$$

When this is inserted in (3.49), the first term gives the mean field and the second term yields the collision term (in the limit of times $t - t_0$ larger than the collision time). We will symbolically write

$$\left(\partial_t - L_1^{\mathrm{HF}}\right) f_1(x_1, t) = C + F(x_1, t),\qquad (3.53)$$

where C is the collision term. Computing F is as difficult as solving the A-body problem. The idea, formulated by Bixon and Zwanzig [20] and adopted by many authors [21–24] is that this term is varying very quickly on a time scale equal to the collision time and that it can be considered as a fluctuating term (as in the Langevin equation). One generally supposes that F is local in space and that its correlations are given by

$$\overline{F(x_1, t) F(x', t')}^{\tau} = \mathcal{F}(\mathbf{p}, \mathbf{p}', \mathbf{r}) \delta(\mathbf{r} - \mathbf{r}') \delta(t - t').\qquad (3.54)$$

It can be shown that $\mathcal{F}$ is equivalent to the sum of the gain and loss terms entering C. This is intuitively plausible, as the more important the collisions are, the larger the fluctuations should be. In practice, the fluctuating term is applied to the lowest moments of the distribution function, which is so redefined after different time steps in order to reproduce this fluctuating changes [21, 25].

   In principle, these fluctuations are contained in the numerical methods of the second kind, as the collision term is simulated stochastically and all correlations as those of the last term in (3.52) are automatically included. More fluctuations may be introduced when the mean field is calculated with the one-body distribution function inside the event as in QMD [27] (although using Gaussian profile functions reduces these fluctuations considerably). To our knowledge, no investigation has been done on the relationship between all these kinds of fluctuations. At low energy (GANIL), it is necessary to have a good description of the fluctuations [24], as they can become critical in the "gas-liquid" instability zone. At high energy (central collisions in the BEVALAC regime), it seems that the methods of the second kind reproduce rather well the observed fluctuations [26], which turn out to be typical thermal fluctuations.
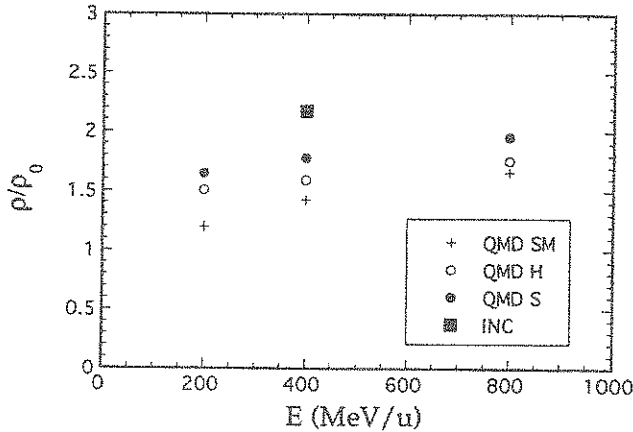
Fig. 5. — Maximum density reached in Au+Au collisions, according to QMD calculations [27] and intranuclear cascade calculations (this work). See text for detail.

3.3. THEORETICAL RESULTS

3.3.1. Preliminaries. — With a "good" transport equation, it is hopefully possible to extract the equation of state by comparing theoretical predictions with data. One is far from this ideal scheme, however, for several reasons:

(i)   we have indicated the present deficiencies of the transport theory and of the methods for solving the tractable transport equations;

(ii) one does not know (without a model) which range of the variables (ρ, T) is probed during a heavy-ion collision;

(iii) the equation of state is not the only "input" of the transport equation;

(iv) it is not obvious to single out the observables which are sensitive to the equation of state and less sensitive to medium effects and, perhaps, to the chosen transport model.

3.3.2. Equation of State. — The observables which have been considered to extract the equation of state (or at least to study their sensitivity to the equation of state) are the flow, the flow angle, the pion multiplicity, the kaon multiplicity and, to a lesser extent, some properties of the multifragmentation. For most of the results, we base our discussion on the QMD review of reference [28], but other and later investigations give similar results.

First, the maximum density reached by the system Au+Au is given by Figure 5, for three QMD calculations. In this context, it is customary to parameterize the equation of state in a (perhaps too much) simplified form, basically a quadratic function of the density, with a second derivative (basically the compressibility) which may be large (hard equation of state, H in Fig. 5) or small (soft equation of

state S). Sometimes equations of state based on velocity dependent effective forces (Eq. (3.41)) are used (SM in Fig. 5). Figure 5 shows that the range of densities that are probed is not very broad and that momentum-dependent forces give less compression, *i.e.* more repulsion.

We now try to summarize the most meaningful results. The flow, either defined by the slope at mid rapidity or by the mean transverse momentum in the reaction plane, is rather sensitive to the equation of state. This is especially true at low energy and the so-called balance point, *i.e.* the incident energy where the flow is changing sign, has been suggested as a good testing quantity for the equation of state. However, very soon, it was realized that this quantity is also very sensitive to medium effects [29]. Moreover, it is also rather sensitive to the experimental filter [30]. Although some authors have claimed that a hard equation of state is necessary, it seems now that the flow up to 400 MeV/u and the position of the balance point could be well-reproduced (without medium effects) with an equation of state based on reasonable momentum-dependent effective interactions [31,32], generating an effective mass of 0.7 and a "soft" equation of state with a compressibility $K \approx 210$ MeV.

Squeeze-out emission [33,34], *i.e.* the preferential emission out of the reaction plane seems to have a good sensitivity to the equation of state but also to the experimental filter. The rapidity distribution shows only a weak dependence upon the equation of state.

The situation concerning the multifragmentation observables is still rather confuse. It is largely believed that multifragmentation is linked to the properties of nuclear matter at small density and small temperature. However, it seems that the production of fragments (in QMD) results mainly for the survival of initial correlations [28,35]. In particular, the origin of the fragments depends upon their mass. As a consequence, the velocity distribution also depends upon the mass and the flow of fragments is different from the flow of protons. According to [28] the flow is larger when the equation of state is harder. However, no detailed investigation of the sensitivity to medium effects and to experimental filters has been done.

The multiplicity of produced mesons (π and K) have been proposed as good probing quantities for the equation of state. The argument is that they are basically produced by thermal motion and are thus sensitive to the amount of compression. Pion yield seems rather insensitive to the equation of state, presumably because reabsorption is quite important. Kaon yield is more sensitive to the equation of state, because these particles are essentially produced below threshold. However, the poor knowledge of the elementary cross-sections [36] and the possible importance of medium effects did not allow to benefit from the good sensitivity to the equation of state, up to now.

3.4. PRODUCED ENTROPY. — This quantity is particularly interesting. It potentially tests the dense matter directly, since it has been shown to remain roughly constant in the expansion phase [37]. In the same reference, a method to measure entropy has been suggested, improving the original method of [38]. It is worth to repeat the argument. One may think that the observed deuterons are formed in

the expansion phase because a proton and a neutron are close to each other in the phase space. The number of deuterons is then given by

$$N_d = 3 \int \frac{\mathrm{d}^3 r \mathrm{d}^3 p}{(2\pi)^3} g_d(\mathbf{r}, \mathbf{p}) \, g_{np}(\mathbf{r}, \mathbf{p}), \qquad (3.55)$$

where g_d is basically the density matrix of the deuteron and g_{np} is the joint probability distribution to find a neutron and a proton at relative distance $\mathbf{r}$ and relative momentum $\mathbf{p}$, with a specific spin orientation (that is assumed to be equally probable as the other ones, hence the absence of an explicit indices for this orientation). One has

$$g_{np}(\mathbf{r}, \mathbf{p}) = \int \frac{\mathrm{d}^3 R \, \mathrm{d}^3 P}{(2\pi)^3} f_2\left(\mathbf{R} + \frac{\mathbf{r}}{2}, \frac{\mathbf{P}}{2} + \mathbf{p}, \mathbf{R} - \frac{\mathbf{r}}{2}, \frac{\mathbf{P}}{2} - \mathbf{p}\right), \qquad (3.56)$$

where the first two variables are relative to the neutron and the remaining ones to the proton. If the two-body distribution function does not vary significantly on the deuteron dimensions and if f_2 can be factorized in a product of f_1's, one gets

$$N_d \approx 3 \int \frac{\mathrm{d}^3 R \, \mathrm{d}^3 P}{(2\pi)^3} f_1\left(\mathbf{R}, \frac{\mathbf{P}}{2}\right) f_1\left(\mathbf{R}, \frac{\mathbf{P}}{2}\right), \qquad (3.57)$$

or

$$N_d = 24\langle f_1\rangle N_{p\uparrow}. \qquad (3.58)$$

Hence

$$R_{dp} = \frac{N_d}{N_p} = 12\langle f_1\rangle, \qquad (3.59)$$

where $\langle f_1\rangle$ is the average of f_1 on itself. On the other hand, the entropy is given by

$$S = -4 \int \frac{\mathrm{d}^3 r \, \mathrm{d}^3 p}{(2\pi)^3} [f_1 \ln f_1 + (1 - f_1) \ln(1 - f_1)]. \qquad (3.60)$$

If $\langle f_1\rangle$ is small, one may replace the second logarithm by $-f_1$ and get

$$\frac{S}{A} = 1 - \langle \ln f_1\rangle. \qquad (3.61)$$

For the Boltzmann distribution, $\langle \ln f_1\rangle$ and $\langle f_1\rangle$ are related by

$$\langle \ln f_1\rangle = \ln\left(\langle f_1\rangle 2^{3/2}\right) - \frac{3}{2}. \qquad (3.62)$$

This relation should hold if f_1 departs, even sizably, from this ideal case, as relation (3.62) deals with global properties of the distribution mainly. From (3.61) and (3.62), one gets

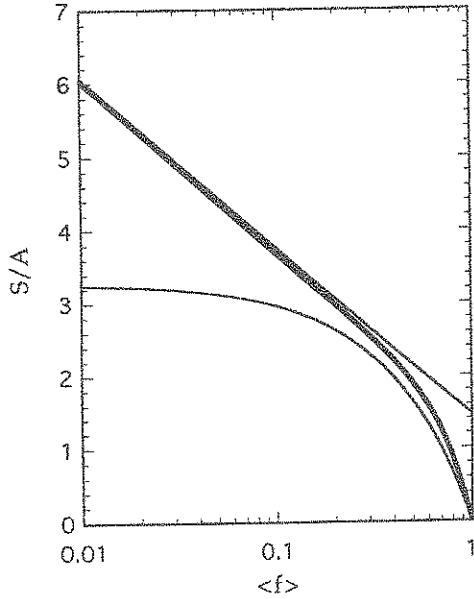$$\frac{S}{A} = 1 + \frac{3}{2}(1 - \ln 2) - \ln\langle f_1\rangle. \qquad (3.63)$$

Fig. 6. — Relation between the entropy per baryon and the mean phase space occupation probability (Eq. (3.67)). See text for detail.

For an almost degenerate Fermi gas, $\langle f_1 \rangle$ is close to unity and this relation is certainly not valid any more. For small T/μ ratio, one has

$$\langle f_1 \rangle \approx 1 - \frac{3}{2}\frac{T}{\mu} \tag{3.64}$$

and

$$\frac{S}{A} \approx \frac{\pi^2}{2}\frac{T}{\mu}, \tag{3.65}$$

which gives

$$\frac{S}{A} = \frac{\pi^2}{3}\left(1 - \langle f_1 \rangle\right). \tag{3.66}$$

The following relation smoothly interpolates between (3.63) and (3.66):

$$\frac{S}{A} = \langle f_1 \rangle \frac{\pi^2}{3}\left(1 - \langle f_1 \rangle\right) + \left(1 - \langle f_1 \rangle\right)\left(1 + \frac{3}{2}\left(1 - \ln 2\right) - \ln \langle f_1 \rangle\right), \tag{3.67}$$

as can be seen in Figure 6. Combining equations (3.59) and (3.67) yields

$$\frac{S}{A} = 3.95 - \ln R_{dp} - 0.053\, R_{dp} - 0.023\, R_{dp}^2 + 0.33\, R_{dp} \ln R_{dp}. \tag{3.68}$$
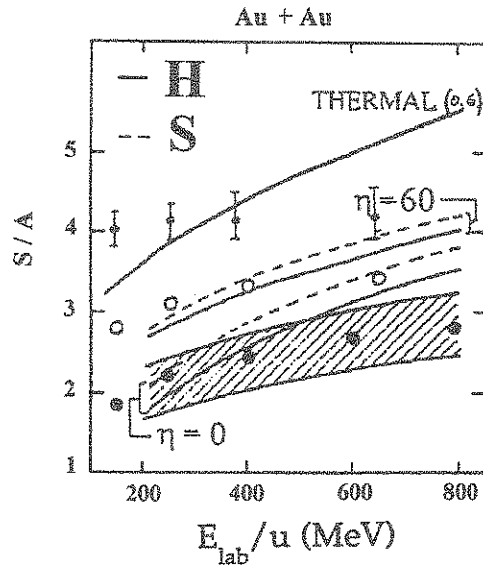
Fig. 7. — Entropy per baryon extracted from the data of reference [34] with the help of equation (3.68) (dots with bars), or with the help of the QSM model (open dots) and extracted from the data of reference [43] with the help of the QSM model (back dots). The shaded area indicates the variation of the results when the freeze-out density is changed from 01. to 0.9 times ρ_0; the upper curve assumes total thermalization. The other full curves correspond to shock waves calculations including or not viscosity (η), and using a hard (full curves) or a soft (dotted curve) equation of state. See text for detail.

Formula of reference [38] reduces to the first two terms. It should be stressed however that the content of the formulae is different. Indeed, the one of [38], as those of the QSM method [39,40], rely on the hypothesis of a thermal and chemical equilibrium between species, whereas formula (3.68) only assumes that neutrons and protons close in phase space at the end of the process simply coalesce. If the system is very dilute (in phase space), the coalescence in real deuterons will dominate. For denser systems, i.e. for increasing $\langle f_1 \rangle$, they will coalesce in larger clusters also. Physically, N_d (Eqs. (3.55)) does not correspond to free deuterons. It is suggested in [37] that formula (3.59) then involves deuteron-like structures $\tilde{d}$, i.e. also the deuterons hidden in heavier clusters (and the same for protons). However (3.68) has limited validity. Nuclear matter calculations show that the appearance of deuterons is inhibited when $\langle f_1 \rangle$ is large [41,42]. Therefore, formula (3.68) may be useful when $\langle f_1 \rangle$ is small only.

3.4.1. Experimental Results and Discussion. — The experimental results are summarized in Figure 7. They are based on the measurements of [34]. It should be noticed that the new measurements of the FOPI collaboration [43] do not provide

additional points as they cannot distinguish protons from deuterons. The measurements of Borderie *et al.* [44] at lower energy correspond to much smaller $\tilde{d}/\tilde{p}$ and, according to equation (3.68), to a larger entropy, which is counter-intuitive. This illustrates the fact that equation (3.68) and, more basically equation (3.59), are not founded when the system is not very dilute in phase space. Presumably, the ratio $\tilde{d}/\tilde{p}$ does not increase steadily when $\langle f_1 \rangle$ increases. We speculate, according to the considerations at the end of Section 3.4.1, that $\tilde{d}/\tilde{p}$ reaches a maximum for some value of $\langle f_1 \rangle$ and further decreases when $\langle f_1 \rangle \to 1$. The near constancy observed in the entropy extracted from the data of [34] with the help of equation (3.68) could be explained by such a flattening of the dependence of $\tilde{d}/\tilde{p}$ upon $\langle f_1 \rangle$ for $\langle f_1 \rangle \geq 0.1$. Therefore, equation (3.68) could be a good "entropometer" for energies larger than 400 MeV/u only. In this region (see Fig. 7), the entropy is slightly smaller than the one of total disorder (fireball, no compression). When the QSM method is used (which is open to criticism, as we explained), the entropy is about one unit smaller. If one compares it with a shock wave calculation, it seems that the entropy is not much sensitive to the equation of state, but more on the viscosity associated with the expansion phase. It seems that the FOPI data can be explained with a vanishing viscosity [45]. However, they do not agree with the Plastic Ball data [34]. In conclusion, it seems that a satisfactory method to extract the entropy in a large range of $\langle f_1 \rangle$ is still lacking.

3.5. DENSE MATTER SIGNALS. — The possibility of identifying direct signals from dense matter has not been really used in this energy domain, although the first experiment on dilepton emission has been done in this domain (see below). It has driven the interest on such signals in the other energy domains covered in this review. Therefore we will treat this aspect in the remaining chapters. Another possible signal is photon production. It seems however that most of the photons are produced by p–n collisions [46]. However, soft photons as well as those of very high energy may have some other origin. For the latter, it is necessary to know the elementary cross-sections with accuracy. Let us finally mention that the πN correlations [47] give evidence for the formation of Δ-resonances, as suggested in [48].

4. From BEVALAC to AGS Energies

As we have indicated in Section 2, no discontinuities are expected when moving from BEVALAC to AGS energies. The most noticeable aspect is the more and more copious production of other particles than nucleons. We will briefly discuss here the mesonic degrees of freedom, putting in evidence the open problems of this chapter.

4.1. Static Properties of Hadronic Matter

4.1.1. Ideal Gas Thermodynamics. — For ideal quantum gases, the energy density, the density and the entropy density are respectively given by

$$
\epsilon = \frac{g}{2\pi^2} T^4 \left(\frac{m}{T}\right)^2 \sum_{\ell=1}^{\infty} \frac{3K_2\left(\frac{\ell m}{T}\right) + \frac{\ell m}{T} K_1\left(\frac{\ell m}{T}\right)}{\ell^2} (\delta)^{\ell-1} \exp\left(\frac{\ell\mu}{T}\right), \qquad (4.1)
$$

$$
n = \frac{g}{2\pi^2} T^3 \left(\frac{m}{T}\right)^2 \sum_{\ell=1}^{\infty} \frac{K_2\left(\frac{\ell m}{T}\right)}{\ell} (\delta)^{\ell-1} \exp\left(\frac{\ell\mu}{T}\right), \qquad (4.2)
$$

$$
\sigma = \frac{g}{2\pi^2} T^3 \left(\frac{m}{T}\right)^2 \sum_{\ell=1}^{\infty} \frac{\left(4 - \frac{\ell\mu}{T}\right) K_2\left(\frac{\ell m}{T}\right) + \frac{\ell m}{T} K_1\left(\frac{\ell m}{T}\right)}{\ell^2} (\delta)^{\ell-1} \exp\left(\frac{\ell\mu}{T}\right),
$$

$$
(4.3)
$$

where g is the degeneracy factor, m is the mass of the particles, μ is the chemical potential and where

$$
\delta = \begin{cases} +1 & \text{bosons} \\ 0 & \text{boltzmannions} \\ -1 & \text{fermions} \end{cases} \qquad (4.4)
$$

It is interesting to mention their value in some limits. If $\frac{m}{T} \gg 1$ and $m - \mu \gg T$, one has, irrespectively of the statistics

$$
\epsilon = gm \left(\frac{mT}{2\pi}\right)^{3/2} e^{-\frac{m-\mu}{T}} \left(1 + \frac{27}{8}\frac{T}{m} + ...\right) \qquad (4.5)
$$

$$
n = g \left(\frac{mT}{2\pi}\right)^{3/2} e^{-\frac{m-\mu}{T}} \left(1 + \frac{15}{8}\frac{T}{m} + ...\right) \qquad (4.6)
$$

$$
\sigma = g \left(\frac{mT}{2\pi}\right)^{3/2} e^{-\frac{m-\mu}{T}} \left(\frac{m-\mu}{T} + \frac{35}{8} + ...\right), \qquad (4.7)
$$

and

$$
\epsilon = n \left(m + \frac{3}{2}T\right), \qquad (4.8)
$$

i.e., one recovers the non relativistic non degenerate gas limit. If $\frac{m}{T} \ll 1$ and $\mu = 0$, one has

$$
\epsilon = g\frac{\pi^2}{90}T^4 \quad , \quad n = 1.11 \, g\frac{\pi^2}{90}T^3 \quad , \quad \sigma = 4g\frac{\pi^2}{90}T^3 \qquad (4.9)
$$

for bosons and

$$
\epsilon = \frac{7}{8}g\frac{\pi^2}{90}T^4 \quad , \quad n = 0.729 \times \frac{7}{8}g\frac{\pi^2}{90}T^3 \quad , \quad \sigma = \frac{7}{2}g\frac{\pi^2}{90}T^3 \qquad (4.10)
$$

for fermions. In the latter case, n indicates the number of fermions and antifermions.
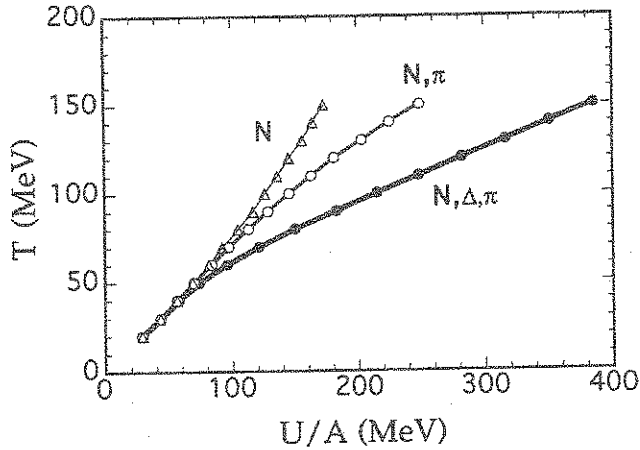
Fig. 8. — Relation between temperature and energy for a gas of nucleons, of nucleons and pions, of nucleons, Δ's and pions, respectively.

The main effect of mesonic and baryonic resonance production can be studied in a very simple model. Let us consider a mixture of nucleons, Δ's and pions, resulting from the heating of a system of A nucleons in a volume V. The parameters entering equations (4.5–4.7) to simplify, i.e. the chemical potentials μ_N, μ_Δ, μ_π and the temperature T can be determined from the total energy and the baryon number

$$U = V \left(\epsilon_{\rm N} + \epsilon_\Delta + \epsilon_\pi \right) + U_0 \tag{4.11}$$

$$A = V \left(n_{\rm N} + n_\Delta \right), \tag{4.12}$$

and the relations between the chemical potentials

$$\mu_\Delta = \mu_{\rm N} \quad , \quad \mu_\pi = 0, \tag{4.13}$$

resulting from the reactions NN $\rightleftharpoons$ NΔ, $\Delta \rightleftharpoons$ Nπ governing the equilibrium. In equation (4.11), U_0 is the compression energy. The variation of the temperature (for the case $A = 200$, $V = 800$ fm^3) is given in Figure 8. The temperature is increasing much more slowly with the available energy when resonance production is switched on. Physically, this corresponds to the fact that energy is more and more transformed into mass rather than in random motion. Correlatively, an excess of entropy is produced. It is easy to imagine that other types of resonances will amplify the phenomenon. Hagedorn [49] has shown that this leads to the existence of a limiting temperature. For a system of mesons (the argument can be reproduced for baryons), one has

$$\epsilon = \frac{3T^2}{2\pi^2} \int_0^\infty dm \rho(m) \ m^2 \ K_2 \left(\frac{m}{T} \right), \tag{4.14}$$

where the dominant Boltzmannian contribution has been retained for simplicity, and where $\rho(m)$ is the mass spectrum density. Heavy mesons being made of lighter ones (statistical bootstrap hypothesis), $\rho(m)$ obeys the equation

$$\rho(m) = \delta(m - m_\pi) + \sum_{n=2}^{\infty} \frac{1}{n!} \int \delta\left(m - \sum_{i=1}^{n} m_i\right) \prod_{i=1}^{n} \rho(m_i) \, dm_i. \qquad (4.15)$$

If m is very large and if one retains the $n = 2$ term, $\rho(m) \approx \rho(m_1)\rho(m - m_1)$, whose solution is an exponential

$$\rho(m) = \exp(\alpha m). \qquad (4.16)$$

It turns out that the solution of (4.15) is close to (4.16) for large m and $\alpha \approx m_\pi^{-1}$. The energy density (4.14) diverges when $T \to \alpha^{-1}$, because of the behaviour of the K_2 function. The measure of the specific heat would be a check of this model and of the meson spectrum. The Hagedorn model has been viewed sometimes as an elegant way to account for interactions between pions. However, it should be reminded that in this model, the pressure follows the ideal gas law $p = nT$. The model should break down at some temperature, because quark degrees of freedom should enter the scene (see Sect. 5). It has been sometimes speculated that the limiting temperature coincides with the hadronic to quark matter transition.

4.1.2. Models for Interacting Mesons. — Generalizing the $\sigma - \omega$ model of Walecka [50], a broad class of models have been proposed. The starting point is a Lagrangian density of this kind:

$$\mathcal{L} = \sum_{B} \overline{\psi}_B \left(i\gamma_\mu \partial^\mu - m_B + g_{\sigma B}\sigma - g_{\pi B}(\partial_\mu \pi) \cdot (\gamma_5 \gamma^\mu \tau)\right.$$

$$\left. -g_{\omega B}\gamma_\mu \omega^\mu - \frac{1}{2} g_{\sigma B}\gamma_\mu \tau_3 \rho_3^\mu \right) \psi_B + \frac{1}{2}\left(\partial_\mu \sigma \partial^\mu - m_\sigma^2 \sigma^2 + U(\sigma)\right)$$

$$\qquad (4.17)$$

$$+ \left(\partial_\mu \pi . \partial^\mu \pi - m_\pi^2 \pi^2\right) - \frac{1}{4} \omega_{\mu\nu}\omega^{\mu\nu}$$

$$+ \frac{1}{2} m_\omega^2 \omega_\mu \omega^\mu - \frac{1}{4} \rho^{\mu\nu}\rho^{\mu\nu} + \frac{1}{2} m_\rho^2 \rho_\mu \rho^\mu.$$

We will not detail all the terms of this Lagrangian. The σ-field self-energy has the form

$$U(\sigma) = \frac{b}{3} \sigma^3 + \frac{c}{4} \sigma^4 \qquad (4.18)$$

and is chosen so to stabilize the system. For a uniform matter at rest, all meson fields are constant, except the pion field, which has the form

$$\pi = \frac{\overline{\pi}}{\sqrt{2}} e^{ikx}, \qquad (4.19)$$

because of the derivative coupling. The equations of motion write

$$m_\sigma^2 \sigma_0 = g_{\sigma_B} \langle \bar{\psi}_B \psi_B \rangle - \frac{dU}{d\sigma} \qquad (4.20)$$

$$m_\omega^2 \omega_0 = g_{\omega_B} \langle \bar{\psi}_B \gamma_0 \psi_B \rangle \qquad (4.21)$$

$$\left(m_\rho^2 + (g_\rho \bar{\pi})^2 \right) \rho_0 = g_{\rho_B} \langle \bar{\psi}_B \tau_3 \gamma_\mu \psi_B \rangle \qquad (4.22)$$

$$\left(-k_\mu k^\mu + m_\pi^2 \right) \bar{\pi} = -g_{\pi_B} \langle \bar{\psi}_B \gamma_5 \gamma_\mu k^\mu \tau \psi_B \rangle \qquad (4.23)$$

and

$$\left\{ \gamma_\mu \left(\partial^\mu - g_{\omega_B} \omega^\mu \right) - (m - g_{\sigma_B} \sigma) + \gamma_\mu k^\mu \left(\frac{\tau_3}{2} + g_{\pi_B} \bar{\pi} \gamma_5 \tau_2 \right) \right\} \psi_B = 0. \qquad (4.24)$$

The coupling gives a non vanishing value to some fields and provides the baryon with an effective mass and an effective momentum. Most of the time, the authors calculate the single-particle energies $e(k)$ and use them as the basic ingredient for thermodynamics. One gets

$$\epsilon = \frac{1}{2} m_\sigma^2 \sigma_0^2 + U(\sigma_0) + \frac{1}{2} m_\omega^2 \omega_0^2 + \frac{1}{2} \bar{\pi}^2 \left(k_\mu k^\mu + m_\pi^2 \right) + \frac{1}{2} m_\rho^2 \rho_0^2$$

$$+ \sum_B \int \frac{d^3 p}{(2\pi)^3} \frac{e(p)}{1 + \exp \frac{e(p) - \mu}{T}} \qquad (4.25)$$

$$p = -\frac{1}{2} m_\sigma^2 \sigma_0^2 - U(\sigma_0) + \frac{1}{2} m_\omega^2 \omega_0^2 + \frac{1}{2} m_\rho^2 \rho_0^2 + \frac{1}{3} \sum_B \int \frac{d^3 p}{(2\pi)^3} \frac{p^2}{e(p)} \frac{1}{1 + \exp \frac{e(p) - \mu}{T}} . \qquad (4.26)$$

The number of mesons is given by the square of the corresponding field. A problem appears readily: for matter at rest, the pion field exists only for $k = 0$. Therefore, quite often, these models are utilized for the baryon sector only, ideal gas formulae being used for mesons [51, 52].

4.1.3. *Chiral Models.* — Here, we anticipate a little bit on Section 5, considering the pion as the Goldstone boson related to the spontaneous breaking of chiral symmetry. The most popular model is the one initially created by Nambu and Jona-Lasinio [53]. We will follow here a modern formulation, presented in [54]. The starting point is the Lagrangian density

$$\mathcal{L} = \bar{\psi} \left[i \gamma_\mu \partial^\mu - m - g \left(\sigma + i \gamma_5 \tau \cdot \pi \right) - \Gamma_a \varphi_a \right] \psi + \mathcal{L}_{\varphi_a} + \frac{1}{2} a^2 \left(\sigma^2 + \pi^2 - f_\pi^2 \right)^2 , \qquad (4.27)$$

where φ_a stands for the other meson fields. As in the preceding models, the mesons fields are treated classically. The thermodynamics of such a model can be advantageously studied from the partition function

$$Z = \int \mathcal{D} \{ \phi_\alpha \} \exp \left[-I_{\text{eff}} \right] , \qquad (4.28)$$

where $\{\phi_\alpha\} = \varphi_a, \sigma$ and π and where

$$
I_{\text{eff}} = - \int_0^\beta \mathrm{d}\tau \int \mathrm{d}^3 r \Big[\mathrm{tr} \ \ln \left\{ i \left(\not{\partial} + \mu\gamma_0 \right) + m + g \left(\sigma + i\gamma_5 \tau \cdot \pi \right) + \Gamma_a \varphi_a \right\}
$$
$$
+ \mathcal{L}_{\varphi_a} + \frac{1}{2} \, a^2 \left(\sigma^2 + \pi^2 - f_\pi^2 \right) \Big],
$$
(4.29)

β and μ being the inverse temperature and the fermion chemical potential. The fermion fields have been integrated out in (4.29). They do not appear anymore as dynamical variables. This procedure is known as the bosonization. We will concentrate here on the chiral field and, thus for the sake of simplicity, we will leave out the φ_a-fields for the moment. The effective action I_{eff} (4.29) can be expanded by making $\phi_\alpha = \phi_\alpha^0 + \delta\phi_\alpha$, where ϕ_α^0 is the value of the fields making the action stationary

$$
I_{\text{eff}} = I_{\text{eff}}^0 + I_{\text{eff}}^1 + I_{\text{eff}}^2.
$$
(4.30)

The stationary condition gives at $T = 0$

$$
\varphi_\alpha^0 = 0, \pi^0 = 0
$$

$$
a^2 \left(1 - \frac{m}{M} \right) = \int \frac{\mathrm{d}^4 k}{(2\pi)^4} \frac{1}{(k - \mu)^2 + M^2},
$$
(4.31)

where $M = m + g\sigma^0$. The integral (4.31) displays an ultraviolet divergence. It should be regularized. At $T \neq 0$, the substraction of the $T = 0$ contribution can be used as a regulator; this yields

$$
a^2 \left(1 - \frac{m}{M} \right) = - \int \frac{\mathrm{d}^3 k}{(2\pi)^3} \frac{1}{k^2 + M^2} \left(n_{i+} + n_{i-} \right),
$$
(4.32)

where

$$
n_{i\pm} = \left\{ 1 + \exp \left[\beta \left(\sqrt{k^2 + M^2} \pm \mu \right) \right] \right\}^{-1}.
$$
(4.33)

Equation (4.31) is called the gap equation, as it gives a mass M (instead of m, which vanishes when the Lagrangian is chirally symmetric) to the fermions. The chiral symmetry is spontaneously broken, which is also reflected in the non vanishing order parameter

$$
\langle \overline{\psi}\psi \rangle = \frac{M}{2} \int \frac{\mathrm{d}^3 k}{(2\pi)^3} \frac{1}{k^2 + M^2} \left(n_{i+} + n_{i-} \right).
$$
(4.34)

The second order contribution I_{eff}^2 can be written as [54]

$$
I_{\text{eff}}^2 = I_{\sigma\sigma}^2 + I_{\pi\pi}^2
$$
(4.35)

with

$$
I_{\sigma\sigma}^2 = \frac{1}{2\beta} \int \mathrm{d}q \ \tilde{\sigma}(q) \, K_{\sigma\sigma}^{-1}(q) \ \tilde{\sigma}(q),
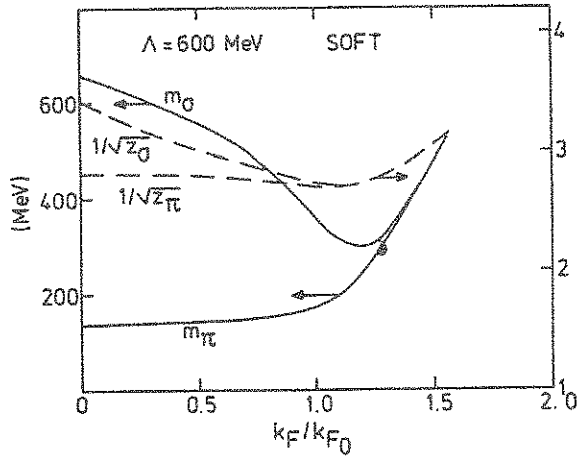$$
(4.36)

Fig. 9. — The full curves give the modification of the π and σ mesons inside nuclear matter, as predicted by a Nambu–Jona-Lasinio model. The quantity k_F is the Fermi momentum and k_{F_0} is the same quantity at normal nuclear matter density. Adapted from reference [54].

where $\tilde{\sigma}(q) = \int d^4 x e^{iqx} \, \delta\sigma(x)$, and a similar expression for $I^2_{\pi\pi}$. The quantities $K_{\sigma\sigma}(q)$ and $K_{\pi\pi}(q)$ are the σ- and π-meson propagators. A non trivial prediction of this kind of model is that the mass of the mesons (i.e. $K^{-1}_{\sigma\sigma}(q^2 = 0)$, $K^{-1}_{\pi\pi}(q^2 = 0)$) is not constant, but varies with the temperature and the chemical potential.

We did not specify the fermion fields. They are usually taken as quark fields, although the model is applied to hadronic matter as well. The "justification" lies in the general belief that chiral symmetry breaking is more important than confinement when global properties of matter are considered.

These models predict nevertheless a phase transition toward a restoration of chiral symmetry at high temperature and high density. In this phase, the fermions recover a small mass, characteristic of a deconfined quark-gluon plasma. The mass of the chiral mesons becomes equal in this phase. The change of these masses with increasing density (at $T = 0$) is shown in Figure 9.

The thermodynamics of this model has not been studied in the mesonic sector, at least with the introduction of the full complexity of the different families of mesons.

4.2. TRANSPORT THEORY. — The models described in Section 4.1 have been used in tentatives to derive transport equations including the creation and destruction of mesons. Detailed works are quite often limited to the relativistic Vlassov (collisionless) equation [55, 56]. There have been several works aiming at deriving a transport equation in the collision regime [57–60], but the most advanced work is the one of [61] using the σ–ω Walecka model. The authors arrive at equations

similar to (3.17) for each of the species (N, σ, ω), the coupling between these equations arising from the "self-energies" $\Sigma^>$ and $\Sigma^<$. However, all these equations are not really numerically tractable. In practice, Boltzmann type equations are used, including reactions between species in the collision term. For instance, for nucleons and pions, these equations write

$$\left(\frac{\partial}{\partial t} - L_N\right) f_N(\mathbf{r}, \mathbf{p}) =$$

$$C^{NN} - \int (dp) \, |T(NN \to NN\pi)|^2 \, f_N(p) \, f_N(p') \, \overline{f}_N(p'') \, \overline{f}_N(p''') \, \overline{f}_\pi(p^{iv}) \qquad (4.37)$$

$$+ \int (dp) \, |T(NN\pi \to NN)|^2 \, f_N(p'') \, f_N(p''') \, f_\pi(p^{iv}) \, \overline{f}_N(p) \, f_N(p')$$

$$\left(\frac{\partial}{\partial t} - L_\pi\right) f_\pi(\mathbf{r}, \mathbf{p}) = C^{\pi N}, \qquad (4.38)$$

where C^{NN} is the usual NN collision term, where (dp) stands symbolically for integrations over phase space and where $C^{\pi N}$ is the opposite of the collision term (except C^{NN}) appearing in (4.37). The notation $\overline{f}$ means $1 - f$ for fermions and $1 + f$ for bosons. In general, one uses $\overline{f} = 1$ for bosons. Using $1 + f$ leads to an explosive production of pions [62], akin to a Bose-Einstein condensation, not observed in reality. This amplification is presumably inhibited by two mechanisms: (i) the modification of pion cross-sections in the medium [63]; (ii) $\pi-\pi$ repulsive interactions (in $T = 0$ channel).

4.3. RESULTS. — The survey of the results on meson production in the BEVALAC-AGS regime has been done by Metag [64]. Remarkably enough, the differential (and also integrated when available) cross-sections follow a systematical trend, that can be expressed as

$$\sigma \approx \sigma_R \, A_{\text{part}} \exp \frac{E_{\text{avail}} - E_{\text{prod}}}{E_0}, \qquad (4.39)$$

where E_{avail} is the available energy NN c.m. energy with the same kinematics as the incoming nuclei, E_{prod} is the production threshold for the NN system, A_{part} is the average number of participant nucleons, and E_0 is a universal constant of the order of 80 MeV. If this behaviour strongly suggests that the mesons are produced by the thermal motion of the nucleons [65], there is no explanation of the universal value of E_0, except perhaps the possible dominance of the Δ-resonance. The theoretical situation is rather unclear. It seems that the BUU calculations of the Giessen group can reproduce the data, at the expense, however, of using modified coupling constants for mesons [66]. Moreover, it seems that these results are somehow sensitive to the equation of state.

It should be mentioned also that, at the AGS energies, a good reproduction of the data can be achieved by the intranuclear cascade code ARC [67], which introduces N^* and Δ resonances, provided (reasonable) assumptions on the reinteractions of these resonances are introduced.
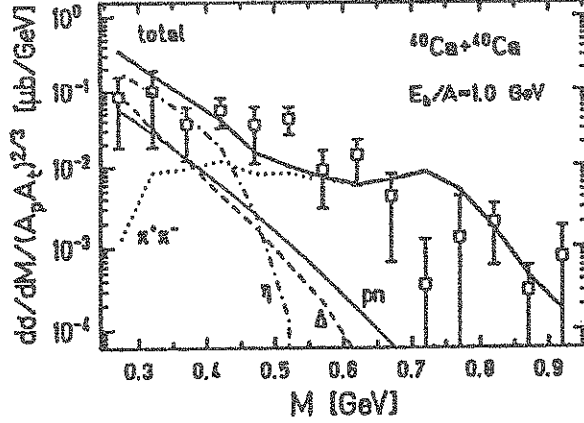
Fig. 10. — Mass spectrum of dileptons in Ca+Ca collisions at 1 GeV/u. Various theoretical contributions are indicated. Adapted from [64].
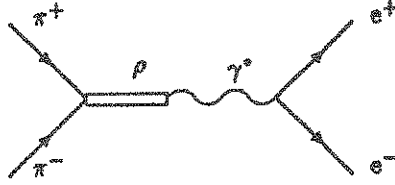

Fig. 11. — Diagram for dilepton production by $\pi^+\pi^-$ collisions in the vector dominance model.

4.4. DILEPTONS. — We pay some attention to this possible signal from the dense phase. There are several sources of dileptons, as indicated by Figure 10. We will come back on some of them in Section 5. We will here only discuss the $\pi\pi$ contribution, corresponding to the graph of Figure 11, assuming that pions are not free, but obeying an in-medium dispersion relation $e(p)$:

$$\frac{d\sigma}{dt} = \frac{e^4}{4\pi} \frac{1}{s^3 \left(s - 4m^{*2}\right)} \left[\frac{s}{2}\left(s - 4m^{*2}\right) - \frac{1}{2}\left(t - u\right)^2\right] \left|F_\pi\left(m_\rho^2\right)\right|^2, \qquad (4.40)$$

with

$$m^{*2} = e(p)\,e(p) - \mathbf{p}\cdot\mathbf{p'}, \qquad (4.41)$$

$$\left|F_\pi\left(m_\rho^2\right)\right|^2 = \frac{m_\rho^4}{\left(s - m_\rho^2\right)^2 + \Gamma_\rho^2 m_\rho^2}. \qquad (4.42)$$

In principle, the dilepton yield may contain some information on the pion dispersion relation inside matter. Figure 10 shows however that, beyond the necessity of having a reliable reaction model, it is essential to know the other contributions with a good precision.
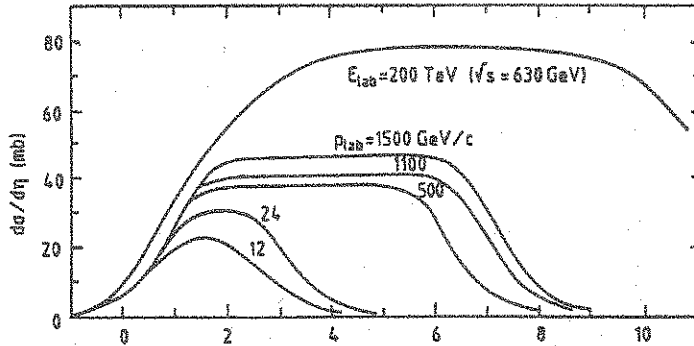
Fig. 12. — Rapidity distribution of produced charged particles in pp collisions at various incident momenta. Adapted from reference [68].

5. Collisions at SPS Energies

5.1. INTRODUCTION. — In contrast to the preceding cases, the ideas on the scenario of the collision are rather vague. It is therefore appropriate to start with nucleon-nucleon collisions at these energies and with the most popular models describing these collisions. Afterwards, we will speak of the quark-gluon plasma and of the theoretical models for heavy-ion collisions. Finally, we will discuss shortly the possible signatures of the plasma.

5.2. NUCLEON-NUCLEON COLLISIONS. — Between $\sqrt{s} = 3$ GeV and $\sqrt{s} = 100$ GeV, the total NN cross-section is of the order of 40 mb and is dominated by the reaction cross-section which amounts to ~30 mb. The reactions can be: (i) diffractive, when one of the nucleons plays the role of an absorptive medium for the other which does not lose much energy, leading to a diffractive pattern at small angle; (ii) non diffractive, where the nucleons lose a lot of energy, leading to a copious production of particles. The latter reactions are the most important ones, covering 80 to 90% of the reaction cross-section. The average charged particle multiplicity is given by

$$\langle N_{\mathrm{ch}} \rangle = 0.88 + 0.88 \ln \sqrt{s} + 0.47 \left(\ln \sqrt{s} \right)^2 . \tag{5.1}$$

These particles show a remarkable momentum distribution. The (pseudo) rapidity distribution has the form of a plateau extending between the two nucleon rapidities, the height of which saturates at about two charged particles per unit of rapidity (see Fig. 12, extracted from the review [68]). The p_{T} distribution is identical for all types of particles when plotted *versus* the variable $m_{\mathrm{T}} = \sqrt{p_{\mathrm{T}}^2 + m^2}$. The average value $\langle p_{\mathrm{T}} \rangle$ is rather small ≈ 0.3 GeV/c. One has to realize anyway that the emission at large $p_{\perp}$ should correspond to a hard process in the perturbative QCD regime. Another important question is the energy loss of the baryons. It seems [69] that
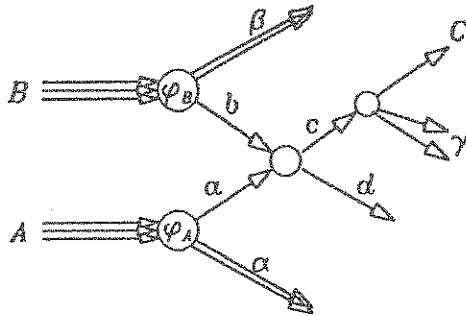
Fig. 13. — Typical diagram for a parton-parton hard scattering process.

the baryons are uniformly distributed in $x_F = p_{\parallel}/p_{inc}$. One can then write

$$\frac{d\sigma}{dy} = \frac{d\sigma}{dx_F}\frac{dx_F}{dy} \propto \frac{d\sigma}{dx_F}\frac{m_{BT}}{m_B}e^{y-y_{inc}} \tag{5.2}$$

when y_{inc} is the rapidity of the incident proton. One finds readily $\langle y \rangle = y_{inc} - 1$, which means that the baryons lose one unit of rapidity on the average.

5.3. PRODUCTION MODELS

5.3.1. Perturbative QCD Model. — The hard scattering model relevant to this regime is illustrated in Figure 13 and implies the interaction of a parton from the projectile with a parton from the target. The partons can be seen as substructures of the nucleon which behave independently of each other when they are probed by a hard scattering (large Q^2) and which carry a given fraction of the nucleon momentum. For simplicity, they can be seen as quarks (valence quarks, as those revealed by the SU(3) model of hadrons, or see quarks) or gluons. The inclusive production cross-section $A + B \rightarrow C + X$ is thus equal to

$$E_C \frac{d^3\sigma}{dC^3}\bigg|_{AB \rightarrow CX} = \sum_{a,b} \int dx_a d^2 a_T \int dx_b\, d^2 b_T\, G_{a/A}(x_a, a_T) G_{b/B}(x_b, b_T) \tag{5.3}$$

$$\times\, r(s, s', x_a, x_b) E_C \frac{d^3\sigma}{dC^3}(ab \rightarrow CX')$$

where the kinematical factor r is roughly equal to unity at high energy. The structure function $G_{a/A}(x_a, a_T)$ is the probability of finding a parton a in particle A, with longitudinal momentum $x_a p_A$ and transverse momentum a_T. The elementary cross-section $E_C \frac{d^3\sigma}{dC^3}(ab \rightarrow CX')$ can be obtained by a perturbative QCD calculation of the relevant diagrams, added with some phenomenological description of the hadronisation of the parton c (see Fig. 13). In some cases, simple estimates can be done. They lead to "counting rules", which rely on some general properties of $G_{a/A}(x)$ for small x

$$G_{a/A}\,\underset{x_a \rightarrow 1}{\sim}\,(1 - x_a)^{g_a}, \tag{5.4}$$

where $g_a = 2n_a - 1$, n_a being the number of spectator "partons" (here taken in the valence sense). Moreover, $E_C \frac{d^3\sigma}{dC^3}$ behaves as

$$E_C \frac{d^3\sigma}{dC^3} \sim \frac{1}{(s')^{n-2}} f(\theta_{CM}) \quad , \quad s' = (p_a + p_b)^2 , \tag{5.5}$$

where n is the number of partons participating to the reaction. This dependence can be guessed on dimensional grounds and is in fact correct in the limit where the mass of the exchanged particle is small compared to s'. Working out the calculations, one easily finds, neglecting transverse motion

$$E_C \frac{d^3\sigma}{dC^3} (AB \rightarrow CX) \underset{x \rightarrow 1}{\sim} (1 - x)^{g_a + g_b + 1} , \tag{5.6}$$

where x is the Feynman variable for the produced particle c. For instance, for π production ab $\rightarrow$ cd corresponds to q$\bar{q} \rightarrow$ q$\bar{q}$, and the cross-section should behave like $(1 - x)^q$, which is confirmed by experiment [70]. Other counting rules hold for the dependence in c_T and for fragmentation processes.

5.3.2. *Production in Strong Fields.* — The idea, first formulated by Schwinger [71], consists in considering the possibility of the creation of particle-antiparticle pairs in strong (Abelian) fields. In QCD, the colour field is non Abelian and confined within the hadrons. When the quark of a meson for instance is pulled from the antiquark, a tube of colour field is stretched between them. The energy contained in this (flux) tube is proportional to the length of the tube, which translates in the linear confining phenomenological potential, and suggests the existence of a uniform field inside the tube. The energy contained in the tube is of the order of $\kappa = 1$ GeV/fm (string constant, see below). The colour field strength $\mathcal{E}$ can be simply evaluated as follows. One has

$$\kappa = \frac{1}{2}\mathcal{E}^2 S, \tag{5.7}$$

where S is the cross-section of the tube. On the other hand, Gauss' law applied to a closed surface including one of the quark gives

$$q = \mathcal{E}S. \tag{5.8}$$

Consequently, one has

$$q\mathcal{E} = 2\kappa, \tag{5.9}$$

where q is the (colour) charge of the quark. When a particle and an antiparticle are created, each of them screens the field seen by the other. In [72], it is argued that the field is reduced by a factor 2. Therefore the potential felt by the created particles along the tube may be written as

$$V(z) = \begin{cases} 0 & z < 0 \\ -\kappa z & 0 < z < L \\ -\kappa L & z > L \end{cases} \tag{5.10}$$
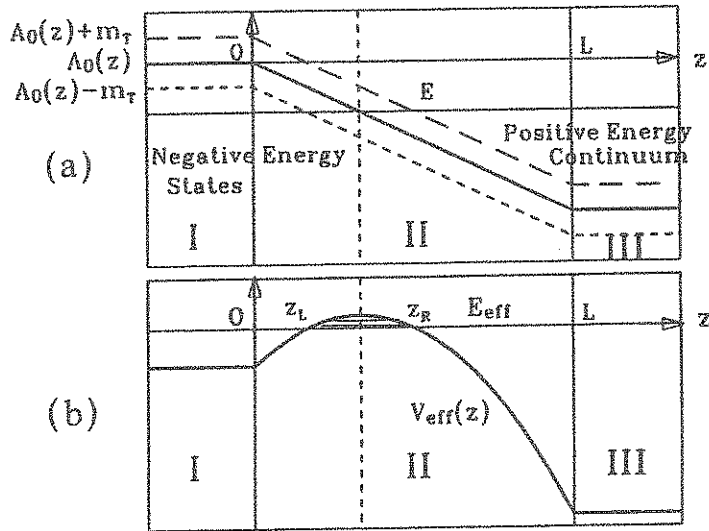
Fig. 14. — Potential $V(z)$ entering equation (5.11); (b) Effective potential entering equation (5.12).

if L is the length of the tube. As it is suggested by Figure 14, antiquarks from the Dirac sea in region I ($z < 0$) are more energetic than the quark in the upper continuum in region III ($z > L$). This is only possible when the length L is sufficiently large $L \geq 2\, m/\kappa$ or $2m_T/\kappa$ if one takes the transverse motion into account. To see that this does correspond really to a tunnelling process, one has to solve the Dirac equation with the potential (5.10). However, it is sufficient to consider the Klein-Gordon equation to exhibit the essential feature. Let us suppose that the transverse mass is fixed for simplicity. One can write

$$\left\{ (E - V(z))^2 - \frac{d^2}{dz^2} - m_T^2 \right\} \psi(z) = 0. \tag{5.11}$$

This equation can be rewritten as a Schrödinger equivalent equation

$$\left\{ \frac{1}{2m_T} \frac{d^2}{dz^2} + \frac{m_T}{2} - \frac{(E - V(z))^2}{2m_T} \right\} \psi(z) = 0. \tag{5.12}$$

The effective potential is quadratic in z and shows two turning points at

$$z_L = \frac{-E - m_T}{\kappa} \quad , \quad z_R = \frac{-E + m_T}{\kappa}. \tag{5.13}$$

They correspond exactly to the points where the horizontal line of energy E crosses the boundaries of the continua. In between, the effective potential is repulsive.

The penetration factor is given, in the WKB approximation, by

$$P = \exp\left\{ -2 \int_{z_\mathrm{L}}^{z_\mathrm{R}} \mathrm{d}z \sqrt{2m_\mathrm{T}\left[\frac{(E - V(z))^2}{2m_\mathrm{T}} - \frac{m_\mathrm{T}}{2} \right]} \right\} = \mathrm{e}^{-\pi\frac{m_\mathrm{T}^2}{\kappa}}. \qquad (5.14)$$

The particle production yield per unit volume and unit time is given by

$$\frac{\mathrm{d}^4 N}{\mathrm{d}^3 x \mathrm{d}t} = \frac{\kappa^2}{(2\pi)^3} \exp\left\{ -\frac{\pi m^2}{\kappa} \right\}. \qquad (5.15)$$

The most striking result of this model is the reduction of production yield with increasing mass of produced particles, arising from the exponential factor in (5.15). In particular, one finds (q = u,d)

$$\frac{N(\mathrm{s}\bar{\mathrm{s}})}{N(\mathrm{q}\bar{\mathrm{q}})} = 0.107 \qquad (5.16)$$

which qualitatively agrees with nucleon-nucleon data. Furthermore, it can be shown that

$$\frac{\mathrm{d}^2 N}{\mathrm{d}p_\mathrm{T}^2} \propto \exp\left(-\pi\frac{p_\mathrm{T}^2}{\kappa} \right). \qquad (5.17)$$

With $\kappa = 1$ GeV/fm, $\sqrt{\langle p_\mathrm{T}^2 \rangle} = \sqrt{\kappa/\pi} \simeq 0.35$ GeV/c, in agreement with the experimental data.

5.3.3. Classical String Model. — The idea that the hadrons can be described as strings comes from the dual resonance model [73], which has been interpreted later on in terms of string scattering [74, 75]. The dual resonance model states that the scattering in the s-channel, where all resonances of spin J should be introduced, is identical to the scattering to all possible exchanges (t-channel exchange). This result can be understood simply if hadrons can be considered as strings. The s- and t-channel scatterings (see Fig. 15) correspond to a single topological diagram, but seen in two different frames. Furthermore, in this model, it has been realized that the exchanged resonances are located on straight lines, named Regge trajectories [76], in the (J, M^2) plane:

$$J(M) = \alpha(0) + \alpha' M^2. \qquad (5.18)$$

It turns out that α' is quasi universal, $\alpha' \approx 1$ GeV^{-2}. Relation (5.18) is characteristic of a rotating string of length $2L$ connecting massless quarks, flying with the velocity of light. Indeed, the mass and the angular momentum of such a system are

$$M = 2 \int_0^L \frac{\kappa \mathrm{d}x}{\sqrt{1 - \left(\frac{x}{L}\right)^2}} = \pi\kappa L \qquad (5.19)$$

$$J = 2 \int_0^L \frac{\kappa x^2 \mathrm{d}x}{\sqrt{1 - \left(\frac{x}{L}\right)^2}} = \frac{\pi}{2}\kappa L^2. \qquad (5.20)$$
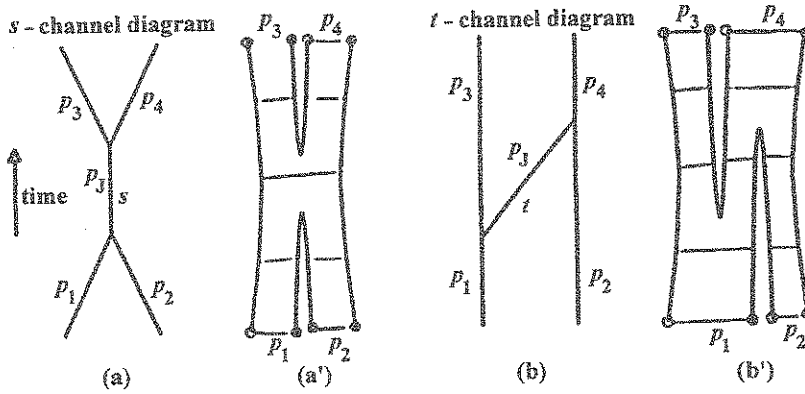
Fig. 15. — Ordinary and string diagrams for the s-channel (left) and t-channel (right) scatterings. Adapted from reference [72].

From these two equations, the following relation is extracted

$$J = \frac{1}{2\pi\kappa} M^2. \tag{5.21}$$

Comparing with (5.18) and $\alpha' \simeq 1$ GeV^{-2}, one extracts $\kappa = 1$ GeV/fm.

The internal dynamics of the string can be described by the Nambu Lagrangian [74]. Here we will use the more simple Hamiltonian form. For a (one-dimensional) string connecting two massless quarks, the Hamiltonian writes

$$H = |p_1| + |p_2| + \kappa \, |x_1 - x_2|. \tag{5.22}$$

The corresponding Hamilton equations are

$$\dot{x}_i = \text{sign } p_i \quad , \quad \dot{p}_i = -\kappa \, \text{sign } (x_i - x_{i'}). \tag{5.23}$$

In the string c.m., the quarks undergo an oscillatory motion with sudden changes of direction (see Fig. 16), denoted as the yo-yo motion with a period $T = 4 |p_1(0)| / \kappa$, where $p_1(0)$ is the initial momentum of the quarks. The trajectories, plotted in the (x, t) plane, form successive squares whose areas are all equal to $\mathcal{A} = s/\kappa^2$. When the string is moving, the trajectories generate rectangles with the same area $\mathcal{A}$, since the latter is an invariant.

Particle production takes place in two steps. First, nucleon-nucleon interactions stretch strings present inside the nucleons. Afterwards, a string may fragment in two new strings. The most popular fragmentation model is the Lund model [77], generalizing the Artru-Mennessier model [78]. The probability that it breaks in a point of space-time, identified by the area A above the first yo-yo point and the rapidity y is given by

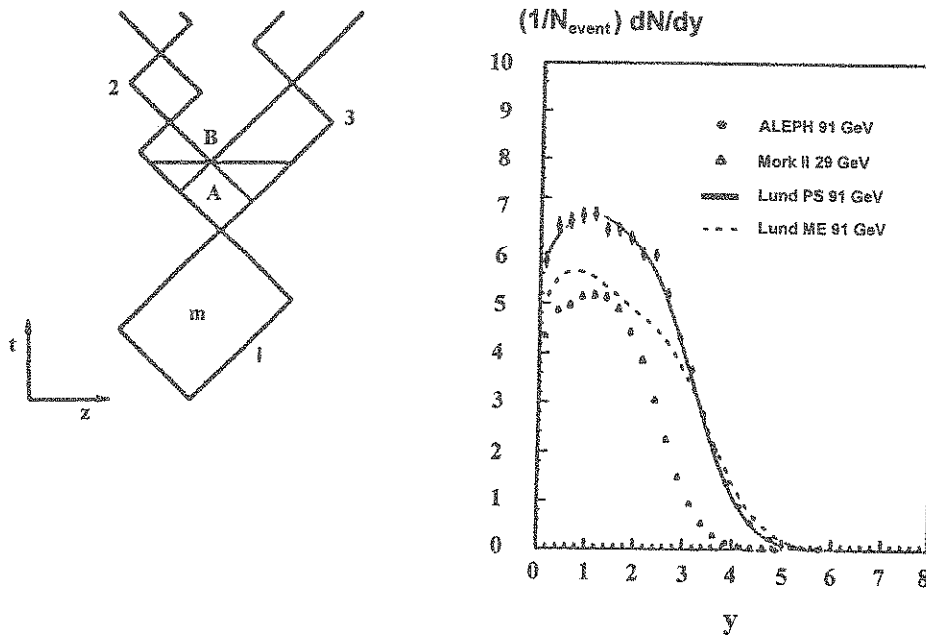$$dP = C \, A^a \, e^{-bA} \, dA \, dy, \tag{5.24}$$

Fig. 16. — Diagram for string fragmentation (lines give the world lines of quarks (see text for detail). The right diagram shows the comparison between the data (dots) and the predictions of the Lund model [77] for rapidity distribution of produced particles.

where C is a normalization constant. Further, each new string may fragment into two strings, *etc.* The probability law for the second fragmentation is strongly influenced by the necessity of having a sequence of fragmentation independent of the frame of reference, as the constancy of dN/dy requires. One has so

$$dP' = Nz_+^{-1} (1 - z_+)^a \ e^{-\frac{bA'}{z_+}}, \qquad (5.25)$$

where z_+ is the fraction of momentum taken by one of the new strings. The strings have a mean lifetime

$$\langle \tau \rangle = \frac{\Gamma\left(a + \frac{3}{2}\right)}{\kappa \sqrt{b} \, \Gamma\left(a + 1\right)}. \qquad (5.26)$$

Figure 15 shows the kind of agreement reached by this model.

5.4. STATIC PROPERTIES

5.4.1. Quark-Gluon Plasma. — The quarks and gluons, which carry colour, are confined in ordinary matter. When the latter is heated (or compressed) sufficiently, these particles are freed. This occurs because the effective coupling between quarks and gluons becomes very small when the typical momentum transfer is large, say

well above 200 MeV [79]. A new state of matter, made of free quarks and gluons is thus expected.

5.4.2. Properties of the Transition. — A simplified model helps to exhibit the transition. For a matter at vanishing baryon number, made of free mesons, the pressure is given by

$$p = g \frac{\pi^2}{90} T^4, \tag{5.27}$$

with $g = 3$. The pressure of an ideal gas of quarks and gluons is

$$p = \left[g_g + \frac{7}{8} \left(q_q + g_{\bar{q}} \right) \right] \frac{\pi^2}{90} T^4 - B = g_{\text{eff}} \frac{\pi^2}{90} T^4 - B, \tag{5.28}$$

where B is the bag constant arising from the fact that an extra energy proportional to the volume of the bag, is needed to produce the perturbative QCD vacuum inside the bag. The value of g_{eff} is 37 (with 2 flavours). The pressure (5.28) is larger (and therefore more favourable) than (5.27) for a sufficiently large temperature, *i.e.* for $T > T_c$, with

$$T_c = \left(\frac{90}{34 \, \pi^2} \right)^{1/4} B^{1/4}. \tag{5.29}$$

If $B^{1/4} = 200$ MeV, as in the MIT bag, $T_c \approx 150$ MeV. Similar considerations can be done at $T = 0$ and non vanishing baryon density.

A tremendous effort has been done in the last years to calculate this transition *ab initio*. It consists in calculating the partition function by discretizing space-time. We will not explain how it is done, avoiding technical points. We refer to the literature for a review (see [72] and Refs. cited therein). The order of the transition is given in Figure 17. It is of first order for gluons only (the pure gauge case), where the internal energy undergoes a sudden change in the transition and approaches the ideal gas value (5.28) in the plasma phase. In this phase the quarks have a small mass, corresponding to the restoration of chiral symmetry. However, the entropy density is sizably smaller than the ideal gas value, indicating that all the degrees of freedom are fully excited. A recent calculation shows that the correlations between quarks disappear very slowly with temperature, which seems to indicate that pions could survive in the plasma [80]. It seems that the physical point in Figure 17, *i.e.* the point corresponding to the actual masses of the u, d and s quarks, corresponds to a second-order phase transition. It should be reminded however that all calculations up to now include fermions in some approximation (the staggered fermions), whose accuracy has not really been established.

5.4.3. Properties of Hadronic Matter. — If plasma is not produced in the ultrarelativistic heavy-ion collisions, the latter may nevertheless produce hadronic matter under extreme conditions. The properties of the latter are not really known. Lattice QCD calculations are of some limited help only, as they can be done in the frame of some approximation only, as we just mentioned. Effective models have been used to investigate this topic. Let us mention the Nambu–Jona-Lasinio type
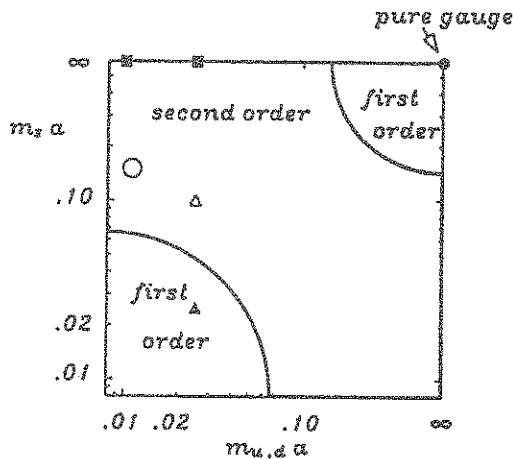
Fig. 17. — Order of the hadron toward quark-gluon plasma phase transition, as predicted by lattice QCD calculations. The m_i, $i = u, d, s$ are the current quark masses and a is the size of the lattice. The circle gives the situation in the real world, *i.e.* to the actual values of the quark masses. Adapted from reference [80].

models for instance. The results of such a model with flavour SU(3) symmetry and gluon background field [81] are summarized in Figure 18 for $\mu_u = \mu_s = 0$. Surprisingly enough, the pressure varies with temperature as T^8 ! Let us finally notice that some authors have tempted to calculate the equation of state of a matter made of strings [82].

5.5. GENERAL FEATURES OF NUCLEUS-NUCLEUS COLLISIONS

5.5.1. Multiple Collisions. — Evidence for multiple collisions undergone by incident nucleons is given by the measurements of the stopping power of incident protons on more and more heavy targets [69, 72, 83]. It should be realized however that the collisions are not independent of each other. As a consequence, one should consider that it is an object of baryon number one which propagates and not necessarily an "asymptotic" proton all the time. The Glauber theory is a nice and simple tool to investigate the number of collisions and the cross-sections. The probability of having collisions at an impact parameter b is given by

$$P(n, \mathbf{b}) = \binom{AB}{n} (T(b) \ \sigma_{in})^n (1 - T(b) \ \sigma_{in})^{AB-n}, \qquad (5.30)$$

where σ_{in} is the inelastic nucleon-nucleon cross-section, where $T(b)$ is the profile function

$$T(\mathbf{b}) = \int d\mathbf{b}_A \int d\mathbf{b}_B \ T_A(\mathbf{b}_A) T_B(\mathbf{b}_B) t(\mathbf{b} - \mathbf{b}_A - \mathbf{b}_B), \qquad (5.31)$$
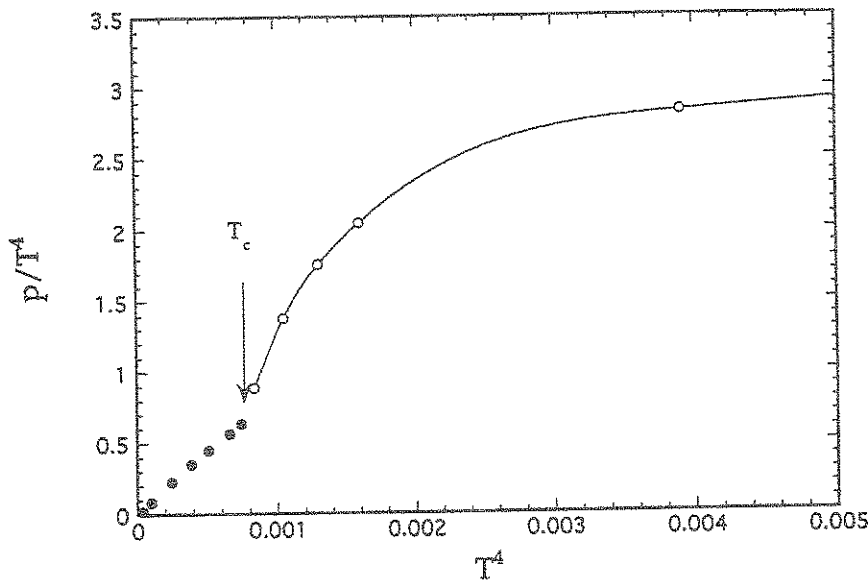
Fig. 18. — Pressure *versus* temperature in a nuclear system at $\mu_u = \mu_s = 0$, as calculated in reference [81].

with

$$T_A(b_A) = \int \rho_A(b_A, z_A)\, dz_A, \tag{5.32}$$

and where t is the "interaction profile", *i.e.* the function which indicates that two particles are passing close enough to each to other to make a collision. For contact interactions, t reduces to a delta function and $T(b)$ is nothing but the overlap between the nuclei's geometrical section weighted by (5.33). In the case the nuclear density has a Gaussian shape, $T(b)$ takes a simple form

$$T(b) = \left(2\pi\, \beta^2\right)^{-1} \exp\left(-b^2/2\, \beta^2\right), \tag{5.33}$$

where β is the Gaussian parameter. From equation (5.31), one finds that the average number of collisions is

$$\langle n(b)\rangle = \sum_{n=1}^{AB} nP(n,b) = ABT(b)\, \sigma_{in}. \tag{5.34}$$

Similarly, one has

$$P(n) = \frac{\int d^2b\, P(n,b)}{\sum_{n=1}^{AB} \int d^2b\, P(n,b)}. \tag{5.35}$$

In the simple case of (5.33), one has

$$
P(n) = \frac{2\pi\beta^2}{\sigma_{\text{in}}^{AB}} \begin{pmatrix} AB \\ n \end{pmatrix} \sum_{m=0}^{AB-n} \begin{pmatrix} AB - n \\ m \end{pmatrix} \frac{(-)^m}{m+n} \left(\frac{\sigma_{\text{in}}}{2\pi\beta^2} \right)^{m+n} , \qquad (5.36)
$$

where σ_{in}^{AB} is the total inelastic cross-section. Its expression can be obtained from (5.36) and the condition $\sum_n P(n) = 1$. When AB is large, (5.31) tends toward a Gaussian shape and $P(n)$ takes the typical form of the observed multiplicity distribution [72] (i.e. a plateau with a steep rise at low multiplicity). This can naturally be explained, as it is expected that the number of produced particles is proportional to the number of collisions.

5.5.2. *Nuclear Stopping Power and Baryon Content.* — There are more and more evidence that, at the SPS, the particles produced at intermediate rapidities are mainly mesons. Baryons are produced at the ends of the available rapidity intervals [72, 84, 85], in contrast to the situation at the AGS [86]. This gave birth to the generally accepted picture of the collision seen in the c.m.: the two nuclei pass through each other, are slightly slowed down and continue their flight by leaving behind a blob of excited matter of vanishing baryon number. Elaborating this idea, Bjorken has proposed an hydrodynamical model, which allows to extract interesting global quantities on the matter produced at intermediate rapidity. Its energy density is given by

$$
\epsilon = \frac{\langle m_{\text{T}} \rangle}{S\tau_0} \frac{\text{d}N}{\text{d}y}, \qquad (5.37)
$$

where S is the geometrical section of this matter, i.e. the section of the intersecting portions of the two partner nuclei (varying with b) and where τ_0 is the proper time necessary for this matter to reach thermalisation. Similarly, the entropy density is given by

$$
s = \frac{3}{S\tau_0} \frac{\text{d}N}{\text{d}y}. \qquad (5.38)
$$

This model does not preclude anything on the nature of this matter. It does assume only that a high degree of equilibration is reached and that matter is expanding self-similarly, which means that there is a one-to-one correspondence between the initial position of a piece of matter at proper time τ_0 and the final rapidity at which the final hadrons in which it decays are detected. Let us however mention that this scenario is not compatible (on the first point) with the string fragmentation scenario that we will mention later on.

5.6. REACTION MODELS

5.6.1. *Introduction.* — The construction of a transport theory based on QCD has not reached the same stage of development as for nucleon matter, mainly because of two serious difficulties: confinement and gauge invariance. Several authors have focused their attention on the plasma phase, where the first difficulty disappears, but with mild success [87, 88]. There are models for the reconfining transition but

most of them are still in their infancy. The most advanced models do not deal with the phase transition in detail, as we will see.

5.6.2. Ideal Plasma Hydrodynamics. — This model was introduced by Bjorken [89]. In one dimension (justified by the fact that the motion is basically longitudinal), the formulation is very simple. As dN/dy is basically constant, it is justified to consider that the thermodynamical quantities do not depend upon the longitudinal variable. Therefore they must depend upon the only remaining invariant, namely the proper time τ. The fundamental equation is

$$\frac{\partial T^{\mu\nu}}{\partial x^{\mu}} = 0, \tag{5.39}$$

with

$$T^{\mu\nu} = (\epsilon + p)\, u^{\mu} u^{\nu} - g^{\mu\nu} p, \tag{5.40}$$

where u is the four-velocity, p the pressure and ϵ the energy density. Multiplying by u_{ν} and using $d\tau^2 = d\left(g_{\mu\nu} x^{\mu} x^{\nu}\right)$, one obtains

$$\frac{\partial \epsilon}{\partial \tau} + (\epsilon + p)\frac{\partial u^{\mu}}{\partial x^{\mu}} = 0. \tag{5.41}$$

With one spatial dimension, $\frac{\partial u^{\mu}}{\partial x^{\mu}} = \frac{1}{\tau}$ and

$$\frac{\partial \epsilon}{\partial \tau} + \frac{\epsilon + p}{\tau} = 0. \tag{5.42}$$

For an ideal gas, $\epsilon = 3p$, and

$$\frac{\epsilon(\tau)}{\epsilon(\tau_0)} = \left(\frac{\tau_0}{\tau}\right)^{4/3} \quad , \quad \frac{T(\tau)}{T(\tau_0)} = \left(\frac{\tau_0}{\tau}\right)^{1/3} \quad , \quad \frac{s(\tau)}{s(\tau_0)} = \frac{\tau_0}{\tau}. \tag{5.43}$$

The lifetime of the plasma is thus given by

$$\tau_c = \left(\frac{T(\tau_0)}{T_c}\right)^3 \tau_0. \tag{5.44}$$

5.6.3. String Fragmentation. — We will dwell a little bit on these models, which are quite successful. We will first discuss briefly the fragmentation mechanism. Taking over the notation of Section 5.3.3 and considering Figure 16, one can show that the light-cone coordinates of the string $p_{\pm} = p_0 \pm p_z$ are equal to the length of the sides of the characteristic rectangle, multiplied by κ. Fragmentation occurs at point B and two strings are generated, in agreement with the energy-momentum conservation. One thus has

$$p_+^{(1)} = p_+^{(2)} + p_+^{(3)} \quad , \quad p_-^{(1)} = p_-^{(2)} + p_-^{(3)}. \tag{5.45}$$

The quantities $p_+^{(3)}$ and $p_-^{(2)}$ being those of the coordinates of B (relative to the yo-yo point), the other ones are automatically determined. The fragmentation probability is often taken as given by the Artru-Mennessier law [78]

$$P = e^{-\alpha_0 A} = e^{-\alpha_0 p_+^{(3)} p_-^{(2)}}, \tag{5.46}$$

where A is the area of the rectangle below point B (relative to the first yo-yo point).

5.6.4. The VENUS Model. — In this model [90, 91], the dynamics of the collision is divided into three parts: string formation, string fragmentation and string reinteraction, leading to hadronization. The number m of strings is determined stochastically according to the probability $\sigma_m/\sigma_{\text{tot}}$, where σ_m is the cross-section for the exchange of m pomerons in the Regge-Gribov theory, similar to the m nucleon-nucleon collision cross-section, (Eq. (5.31)). Strings are fragmented sequentially following the Artru-Mennessier rule. Strings which cross each other can fuse to give a cluster of definite mass. Finally stable hadrons are supposed to be produced from a cluster in a thermal model. Furthermore, the $p_\perp$ motion is given at random at the breaking points. This model can be applied to e^+e^-, NN collisions (on which the (few) parameters are fitted) and nucleus-nucleus collisions.

5.6.5. The Other Models. — A schematic comparison between the existing models is given in Table II. The first interactions can be either due to exchange of colour (due to the pomeron) as in VENUS or to a longitudinal excitation as in FRITIOF, or sometimes complemented by a perturbative QCD calculation as in Section 5.3.1. The fragmentation of strings can follow the law (5.46) or the Feynman-Field law (or the slightly different JETSET procedure) for radiation of hadrons by strings. The last column of Table II indicates the possible rearrangement of the objects issued from fragmentation. Let us note the RQMD and SPACER models which describe the full spatial evolution of the hadrons.

Let us mention that in the HERWIG model, the perturbative QCD phase (interaction of partons) dominates the string phase. The Geiger approach proceeds from the same spirit. The partons are supposed to be confined (or decorrelated) from the beginning and followed in space-time. The equilibration is very fast because of the large number of partons. However, it is possible that small x partons cannot really show up in the collision process because of Lorentz contraction and shadowing effects [102].

5.7. QUARK-GLUON PLASMA SIGNATURES

5.7.1. Dileptons. — Within the plasma, dileptons can be created by $q\bar{q}$ collisions:

$$q\bar{q} \to \gamma^* \to \ell^+\ell^-, \tag{5.47}$$

where γ^* stands for a virtual photon. They are expected to leave the plasma easily. The dilepton can be identified by its invariant mass M and its momentum. The production rate (in a neutral plasma) is given by

$$\frac{\mathrm{d}N}{\mathrm{d}x} = 4\,N_c \sum_f q_f^2 \int \frac{\mathrm{d}^3p_1}{(2\pi)^3} \int \frac{\mathrm{d}^3p_2}{(2\pi)^3} f\,(E_1)\,f\,(E_2)\,\sigma\,(M)\,\nu_{12}, \tag{5.48}$$

where the sum runs over flavours, ν_{12} is the (relativistic) relative velocity, f is the energy distribution of quarks and

$$\sigma\,(M) = \frac{4\pi}{3}\,\frac{\alpha^2}{M^2}\left(1 - \frac{4m_q^2}{M^2}\right)^{-1/2}\sqrt{1 - \frac{4m_q^2}{M^2}}\left(1 + 2\frac{m_q^2 + m_\ell^2}{M^2} + 4\frac{m_q^2 + m_\ell^2}{M^4}\right),$$

$$\tag{5.49}$$

Table II.

Model	First interactions	Fragmentation	Soft/Hard	A-B interaction	Rescattering
VENUS [91]	Color Exchange (Pomeron)	Area law	S/H	Gribov-Regge	Cluster model
DMP (Orsay) [92]	″	j → j + h	S/H	″	—
DPM (DTUJET) [93]	″	″	S/H	″	n-h resc.
QGSM [94]	″	Regge model	S	″	Gribov-Regge
FRITIOF [77]	Longit. Excitation	s → s + h (JETSET)	S	Geometry	—
ATTILA [95]	″	″	S	″	---
PYTHIA [96]	PQCD	″	H	″	---
HIJING [97]	PQCD/FRITIOF	″	S+H	″	—
RQMD [98]	(FRITIOF)	″	S+H	″	h-h resc.
SPACER [99]	(FRITIOF)	s → s + h	S	″	h-h resc.*
HERWIG [100]	PQCD	g → qq̄	H	″	---
GEIGER [112]	PQCD	parton cascade	H	″	---

Working out the integration (5.48) in the case of a (Boltzmann) thermal distribution, one obtains

$$\frac{dN}{dM^2\,d^4x} = 4N_c \sum_f q_f^2\ \frac{\sigma\,(M)}{2\,(2\pi)^4}\ M^2 \left(1 - \frac{4m_q^2}{M^2}\right)^{1/2}\ MTK_1\left(\frac{M}{T}\right). \qquad (5.50)$$

Of course, comparison to experiment requires the integration over the space-time evolution of the plasma. If $M \gg T_0 \gg T_c$, T_0 being the initial temperature of the plasma and an hydrodynamic evolution as in Section 5.6.2, one finds that dN/dM^2 is dominated by

$$\frac{dN}{dM^2} \sim M^{1/2}\ e^{-M/T_0}. \qquad (5.51)$$

Before comparing to experiment, other sources of dileptons have to be considered. They may be active before or after the plasma. Before the plasma, they correspond basically to the Drell-Yan process, in which an incoming parton from the projectile interacts with a parton from the target to create a dilepton as in (5.47). Assuming the production being basically longitudinal, and x_F to be the fraction of initial momentum taken by the dilepton in the NN c.m. frame, one has

$$\frac{d^2\sigma}{dM^2\,dx_F} = \frac{1}{sN_c}\ \sigma\,(M) \sum_f q_f^2\ \frac{q_f^B\,(x_1)\,\overline{q}_f^A\,(x_2) + \overline{q}_f^B\,(x_1)\,q_f^A\,(x_2)}{\sqrt{x_F^2 + \frac{4M^2}{s}}}, \qquad (5.52)$$

with $q_f^B\,(x_1)$ gives the density of quark partons of flavour f with momentum fraction x_1 in nucleus B. For $x_F = 0$ (medium rapidity), one finds that this cross-section depends upon $M/\sqrt{s}$ only. This scaling is found experimentally. One has

$$M^3\ \frac{d^2\sigma}{dM\,dy}\bigg|_{y0} \approx 3 \times 10^{-32}\ e^{-15\ M/\sqrt{s}}\quad \left(cm^2\ GeV^{-2}\right), \qquad (5.53)$$

the power M^3 coming from the transformation $x_F \to y$. In fact (5.52) agrees with the data up to a constant factor K, which can be explained by introducing higher order diagrams, although it is not clear that convergence can be reached. The elementary Drell-Yan cross-section being very small, one has for nucleus-nucleus collisions

$$\frac{d\sigma_{DY}^{AB}}{dM\ dy} \approx AB\ \frac{d\sigma_{DY}^{NN}}{dM\ dy}. \qquad (5.54)$$

The other source of dilepton comes from hadronic collisions after hadronization, as for instance,

$$\pi^+\pi^- \to (\gamma^*, \rho) \to \ell^+\ell^-, \qquad (5.55)$$

where the intermediate ρ is imposed by the vector dominance model. Theoretically, the situation is the same as for (5.47–5.48), provided the adequate quantities are substituted. Cross-section (5.49) then contains the ρ-meson form factor. Finally, one has also to consider the dileptons coming from the decay of mesonic resonances
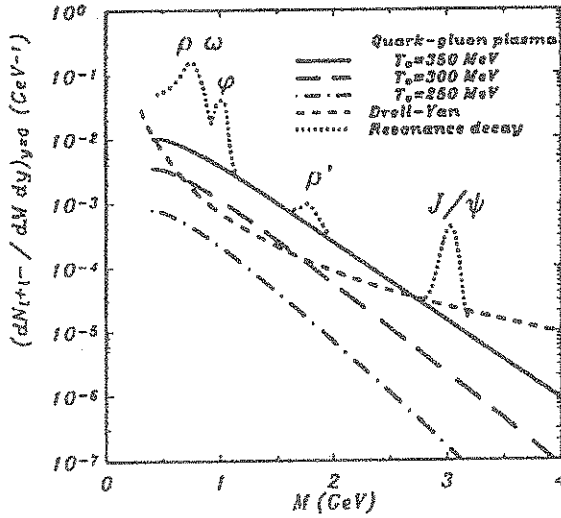
Fig. 19. — Distribution of dilepton mass at zero rapidity splitted in various components. See text for detail. Adapted from reference [72].

(their M spectrum has peaks on the resonance energies). To evaluate this component, one needs a good model for the hadronic phase. The various contributions are depicted in Figure 19. One can see that it will be quite difficult to isolate the plasma component from the other ones [103, 104].

5.7.2. Charmonium Resonances. — Charmonium resonances cannot be produced by charm quarks in the plasma, because there are too few of them. It proceeds only from initial parton-parton collisions. A reduction of the J/ψ and ψ' production [105] (compared to folding of p-nucleus or p–p collisions) is observed, which is presumably due to the interaction of J/ψ with dense matter. Following Matsui and Satz [106], this may be due to Debye screening of colour force between c and $\bar{c}$ quarks, leading to the dissolution of the resonances, in close similarity to ionization of atoms in an ordinary plasma. In the latter case, screening may be understood as follows. Let us assume that a charge q is added to a uniform neutral plasma of density n. The potential generated by this charge is given by

$$\Delta V = -4\pi q\delta(r) + \delta n(r), \tag{5.56}$$

where δn is the modification of density induced by the charge. The latter is constrained by the constancy of the chemical potential over the whole volume of the plasma

$$\mu = \mu(n + \delta n(r), T) + V(r). \tag{5.57}$$

Using the latter relation in first order in δn, one can rewrite equation (5.56) as

$$\Delta V + \frac{\mathrm{d}n}{\mathrm{d}\mu}V = -4\pi q\delta(r).\tag{5.58}$$

The potential takes a Yukawa form instead of the Coulomb force. For colour forces inside the plasma, one finds

$$V = \frac{\mathrm{e}^{-r/r_{\mathrm{D}}}}{r},\tag{5.59}$$

with

$$r_{\mathrm{D}}^{-1} = \sqrt{\frac{N_{\mathrm{c}}}{3} + \frac{N_f}{6}}\,gT,\tag{5.60}$$

g being the coupling constant. If the temperature is larger and larger, the potential is weaker and weaker, and the $c - \bar{c}$ bound states disappear progressively, which qualitatively agrees with experiment [105, 107, 108]. However, one should take account of the fact that J/ψ resonance is not produced directly. In fact, in p—p collisions, what is produced is a wave packet containing a correlated superposition of J/ψ, ψ' and heavier resonances [109–111]. In nucleus-nucleus collisions, it is this wave packet which propagates. Moreover, it has been proven that the J/ψ is produced significantly in a colour octet state, which loses its colour afterwards. This raises the interesting problem of the propagation of a complex coloured object inside a hadronic medium and/or a plasma. In spite of these considerations, a "conventional" explanation has been advanced in [112]. It is based on the ordinary multiple collision picture. Within Glauber theory, the J/ψ production in p-nucleus collisions can be expressed as:

$$\sigma_{J/\psi}^{\mathrm{pA}} = \int \mathrm{d}^2b \int_{-\infty}^{z} \rho\left(b, z'\right)\mathrm{d}z'\,\sigma_{J/\psi}^{\mathrm{pp}}\,\exp\left[-\int_{z}^{\infty}\rho\left(b, z'\right)\sigma_{J/\psi}^{\mathrm{abs}}\right],\tag{5.61}$$

or

$$\sigma_{J/\psi}^{\mathrm{pA}} \approx A\,\sigma_{J/\psi}^{\mathrm{pp}}\left[1 - \overline{L}\rho_0\,\sigma_{J/\psi}^{\mathrm{abs}}\right],\tag{5.62}$$

where

$$\overline{L} \approx \frac{3}{4}R\frac{A-1}{A}.\tag{5.63}$$

For nucleus-nucleus collisions, one obtains

$$\sigma_{J/\psi}^{\mathrm{AB}} \approx AB\,\sigma_{J/\psi}^{\mathrm{pp}}\left[1 - \overline{L}_{\mathrm{AB}}\,\rho_0\,\sigma_{J/\psi}^{\mathrm{abs}}\right],\tag{5.64}$$

with $\overline{L}_{\mathrm{AB}} \approx \overline{L}_{\mathrm{A}} + \overline{L}_{\mathrm{B}}$. Most of the existing data are consistent with formulae (5.62–5.64), provided $\sigma_{J/\psi}^{\mathrm{abs}} \approx 5.2$ mb, which seems definitely larger than the experimental value [113], resulting in fact from indirect measurements. Finally, we want to add that recent measurements on the Pb+Pb collisions at the SPS [114] show a strong departure from this systematics. However, it is not clear that the identification of $\overline{L}_{\mathrm{AB}}$ with a given interval of produced energy transverse is as obvious as it is with largely asymmetric systems (like S + U) studied up to now.

5.7.3. *Hard Photons.* — In the plasma, photons can be produced by $q + \bar{q} \to \gamma + g$ and $g + q\,(\bar{q}) \to q\,(\bar{q}) + \gamma$ processes, which are the equivalents of the annihilation process $(q + \bar{q} \to 2\gamma)$ and Compton scattering $(\gamma + q \to \gamma + q)$ in QED. In fact, the cross-sections are the same up to a coupling constant and a colour factor. For the "annihilation" process, one has with obvious notation

$$E_\gamma \frac{d^3\sigma}{dp_\gamma^3} (q\bar{q} \to \gamma g) = \frac{\alpha_s}{\alpha_e} \left(\frac{e}{q}\right)^2 E_\gamma \frac{d^3\sigma}{d^3 p_\gamma} (q\bar{q} \to \gamma\gamma), \qquad (5.65)$$

where the last cross-section can be obtained from the $e^+ e^- \to \gamma\gamma$ one by simply changing the masses. One finally has

$$\frac{d\sigma}{dt}(q\bar{q} \to \gamma g) = \left(\frac{q}{e}\right)^2 \frac{8\pi\alpha_s\alpha_e}{s\,(s - 4m^2)} \left\{ \left(\frac{m^2}{t - m^2} + \frac{m^2}{u - m^2}\right)^2 \qquad (5.66) \right.$$
$$\left. + \left(\frac{m^2}{t - m^2} + \frac{m^2}{u - m^2}\right) - \frac{1}{4}\left(\frac{t - m^2}{u - m^2} + \frac{u - m^2}{t - m^2}\right) \right\}.$$

The maximum occurs for $\theta_{\gamma q} = 0$ and $\theta_{\gamma\bar{q}} = 0$, *i.e.* when the γ's are produced without significant change of momentum. One can thus write, in a good approximation

$$E_\gamma \frac{d^3\sigma}{d^3 p_\gamma} (q\bar{q} \to \gamma g) \approx \left(\frac{e_q}{e}\right)^2 \sigma_{\text{ann}} \frac{1}{2} E_\gamma \left[\delta\left(\mathbf{p}_\gamma - \mathbf{p}_q\right) + \delta\left(\mathbf{p}_\gamma - \mathbf{p}_{\bar{q}}\right)\right], \quad (5.67)$$

with

$$\sigma_{\text{ann}} = \frac{4\pi\alpha_e\alpha_s}{s - 4m^2} \left\{ \left(1 + \frac{4m^2}{s} - \frac{16m^2}{s^2}\right) \ln\left(\frac{\sqrt{s} + \sqrt{s - 4m^2}}{\sqrt{s} - \sqrt{s - 4m^2}}\right) - \left(1 + \frac{4m^2}{s}\right) \sqrt{1 + \frac{4m^2}{s}} \right\}. \qquad (5.68)$$

Similarly, one has

$$E_\gamma \frac{d^3\sigma}{dp_\gamma^3} (gq \to \gamma q) = \frac{\alpha_s}{\alpha_e} \left(\frac{e}{q}\right)^2 E_\gamma \frac{d^3\sigma}{dp_\gamma^3} (\gamma q \to \gamma q), \qquad (5.69)$$

$$\frac{d\sigma}{dt} (\gamma q \to \gamma q) = \left(\frac{q}{e}\right)^2 \frac{8\pi\alpha_e\alpha_s}{(s - m^2)^2} \left\{ \left(\frac{m^2}{s - m^2} + \frac{m^2}{u - m^2}\right)^2 \qquad (5.70) \right.$$
$$\left. + \left(\frac{m^2}{s - m^2} + \frac{m^2}{u - m^2}\right) - \frac{1}{4}\left(\frac{s - m^2}{u - m^2} + \frac{u - m^2}{s - m^2}\right) \right\}.$$

The maximum occurs for $\theta_{\gamma q} = 0$, as for the ordinary Compton scattering. In first good approximation, one has

$$E_\gamma \frac{d^3\sigma}{dp_\gamma^3} (gq \to \gamma q) \approx \left(\frac{q}{e}\right)^2 \bar{\sigma}_c E_\gamma \, \delta\left(\mathbf{p}_\gamma - \mathbf{p}_q\right), \qquad (5.71)$$

$$\bar{\sigma}_{\rm c} = \frac{2\pi\alpha_{\rm e}\alpha_{\rm s}}{s-m^2} \left\{ \left(1 - \frac{4m^2}{s-m^2} - \frac{8m^4}{(s-m^2)^2} \right) \ln\frac{s}{m^2} + \frac{1}{2} + \frac{8m^2}{s-m^2} - \frac{m^4}{2s^2} \right\}.$$

$$(5.72)$$

Using (5.67) and (5.71) for calculating the yield in a plasma, one gets

$$E_\gamma \frac{{\rm d}N_\gamma^{\rm ann}}{{\rm d}^4x\,{\rm d}^3p_\gamma} = \frac{2N_{\rm s}^2}{(2\pi)^6} \frac{f_{\rm q}({\rm p}_\gamma)}{E_\gamma} \sum_f \left(\frac{q_f}{e}\right)^2 \qquad (5.73)$$

$$\times \int {\rm d}s\,{\rm d}E_{\bar{\rm q}} f_{\bar{\rm q}}(E_{\bar{\rm q}}) \left[1 + f_{\rm g}(E_{\bar{\rm q}})\right] \sqrt{s\,(s-4m^2)}\,\sigma_{\rm ann}(s),$$

and

$$E_\gamma \frac{{\rm d}N_\gamma^{\rm C}}{{\rm d}^3p_\gamma{\rm d}^4x} = \frac{4N_{\rm s}}{(2\pi)^5} \frac{f_{\rm q}({\rm p}_\gamma)}{4E_\gamma} \sum_f \left(\frac{q_f}{e}\right)^2 \qquad (5.74)$$

$$\times \int {\rm d}s\,{\rm d}E_{\rm g}\,f_{\rm g}(E_{\rm g}) \left[1 + f_{\rm q}(E_{\rm g})\right] \left(s-m^2\right) \bar{\sigma}_{\rm c}(s).$$

A theoretical problem appears here. The cross-section (5.72) diverges when $m \to 0$. In a plasma, this divergence seems to be avoided, because interactions are not vanishingly small, because of the large particle density (which increases as T^3). They modify the masses of the quarks. In [88,115,116] it is shown that the effective mass of the quarks is given by

$$m^* = \frac{g}{4\pi}\,\sqrt{\mu^2 + \pi^2 T^2}. \qquad (5.75)$$

Of course, as for dileptons, other γ sources should be considered. They are either hadronic reactions like

$$\pi\pi \to \gamma\rho \quad \text{or} \quad \pi\rho \to \gamma\pi, \qquad (5.76)$$

radiative decays of mesonic resonances (π^0 and η, mainly) and also initial parton-parton collisions. The latter can be evaluated by (5.73) and (5.74) after proper substitution of the quark distribution functions inside the plasma by the nucleus structure functions. For the other ones, a good hadronic scenario is needed. For the moment, the experimental and theoretical uncertainties are such that no clear signal for a radiation by the plasma has been extracted up to now.

5.7.4. *Strangeness.* — When a nuclear system is excited, strange quarks are produced which, in a hadronic phase, will appear in strange hadrons. The $\bar{s}$ quarks will sit inside kaons, essentially. The strange content (for vanishing baryon number) is given by

$$\frac{s}{q} = \frac{s+\bar{s}}{u+\bar{u}+d+\bar{d}} = \frac{K^+}{\frac{3}{2}\,\pi^+ + K^+} = \frac{\frac{K^+}{\pi^+}}{\frac{3}{2} + \frac{K^+}{\pi^+}}, \qquad (5.77)$$

if there is charge symmetry. For a pp system at 14 GeV/c, $s/q \approx 0.05$, which is in fact very close to the value observed in p−Be collision at the same energy [117].

In a thermally equilibrated system, one has

$$\frac{K^+}{\pi^+} \approx \frac{m_{K^+}}{m_{\pi^+}} \frac{K_1\left(\frac{m_{K^\pm}}{T}\right)}{K_1\left(\frac{m_{\pi^\pm}}{T}\right)}. \tag{5.78}$$

For $T \sim 100$ MeV, this yields $s/q \approx 0.2$ and, of course, this ratio increases with temperature. These simple considerations show that strange quark degrees of freedom are far from being saturated in p–p and p-nucleus collisions.

In a plasma (at $B = 0$), chemical equilibrium corresponds to a result similar to (5.78), with the mass of the quarks replacing the one of the mesons, which typically yields $s/q \approx 0.35$. Calculations of [118, 119] indicate that chemical equilibrium could settle very quickly inside the plasma.

Measurements [117] at the AGS shows that K^+/π^+ increases with the mass of the system, which leads to believe that associated production ($\pi N \rightarrow \Lambda K$) is not negligible and/or that the mass of the kaons decreases inside the medium, which lowers the effective kaon production thresholds.

It seems more interesting to study the strange baryon production in the baryon rich domain of rapidity. In purely hadronic reactions, strange antibaryons are strongly suppressed (see the Schwinger factor in model of Sect. 5.3.2). On the contrary, strange and even multistrange antibaryons coming from the cooling of the plasma are not hindered. Experimental results concerning the $\bar{\Xi}/\Xi$ ratio at the SPS [120] shows a definite enhancement in the S+W system, compared to pW, e^+e^- and $\bar{p}p$. However, a detailed investigation of the production in the hadronic phase is still needed before drawing definite conclusions.

6. Summary

We have presented several theoretical questions related to heavy-ion collisions. We have seen that the primordial goal of these studies (good transport theory, helping to extract information on dense matter) is not reached yet, by far. However, this physics should be pursued for the simple reason that the theory of strong interactions (QCD) for extended systems can be studied in the non perturbative sector by this means only, apart from, perhaps, neutron stars and some cosmological constraints. Moreover, we have, here, a perhaps unique case in physics, where the systems can be studied on several (energy and length) scales. The passage from the degrees of freedom relevant at a scale to those relevant at the next scale is far from being understood and will require, without any doubt, an important effort in the next few years.

References

[1] Schulze H.-J., Cugnon J., Lejeune A., Baldo M. and Lombardo U., *Phys. Rev. C* **52** (1995) 2785.
[2] ter Haar B. and Malfliet R., *Phys. Rev. Lett.* **56** (1986) 1237.

[3] Friedman B. and Pandharipande V.R., *Nucl. Phys. A* **361** (1981) 502.

[4] Jeukenne J.-P., Lejeune A. and Mahaux C., *Phys. Rep. C* **25** (1976) 83.

[5] Grangé P., Cugnon J. and Lejeune A., *Nucl. Phys. A* **473** (1987) 365.

[6] Nikhef Annual Report (Nikhef, Amsterdam, 1991) p. 68

[7] Vonderfecht B.E., Dickhoff W.H., Polls A. and Ramos A., *Nucl. Phys. A* **555** (1993) 1.

[8] Jeukenne J.-P., Lejeune A. and Mahaux C., *Nucl. Phys. A* **245** (1975) 411.

[9] Das D., Tripathi R.K. and Cugnon J., *Phys. Rev. Lett.* **56** (1986) 1663.

[10] Kadanoff L.P. and Baym G., Quantum Statistical Mechanics (W.A. Benjamin, New York, 1962).

[11] Danielewicz P., *Ann. Phys.* **152** (1984) 239, 305.

[12] Malfliet R., *Nucl. Phys. A* **545** (1992) 3c.

[13] Bonche P., Koonin S.E. and Negele J.W., *Phys. Rev. C* **13** (1976) 1226.

[14] Köhler H.S., *Phys. Rev. C* **51** (1995) 3232.

[15] Cugnon J., Grangé P. and Lejeune A., *Phys. Rev. C* **35** (1987) 86.

[16] Li G.Q. and Machleidt R., *Phys. Rev. C* **49** (1994) 566.

[17] Abe Y., Ayik A., Reinhard P.G. and Suraud E., Kyoto University preprint, 1995, YITP-95-18;

[18] Bertsch G.F. and Das Gupta S., *Phys. Rep.* **160** (1988) 189.

[19] Balescu R., Equilibrium and Non Equilibrium Statistical Mechanics (John Wiley, New York, 1975).

[20] Bixon M. and Zwanzig R., *Phys. Rev.* **187** (1969) 267.

[21] Ayik S. and Grégoire C., *Nucl. Phys. A* **513** (1990) 187.

[22] Ayik S., Suraud E., Stryjewski J. and Belkacem M., *Z. Phys. A* **337** (1990) 413.

[23] Randrup J. and Rémaud B., *Nucl. Phys. A* **514** (1990) 339.

[24] Chomaz P., Burgio G.F. and Randrup J., *Phys. Lett. B* **254** (1991) 340.

[25] Belkacem M., Suraud E. and Ayik S., *Phys. Rev. C* **47** (1993) R16.

[26] Cugnon J. and L'Hôte D., *Nucl. Phys. A* **452** (1986) 738.

[27] Aichelin J. and Stöcker H., *Phys. Lett. B* **176** (1986) 14.

[28] Aichelin J., *Phys. Rep.* **202C** (1991) 233.

[29] Bertsch G., *et al.*, *Phys. Lett. B* **189** (1987) 384.

[30] Gossiaux P.-B., private communication.

[31] Zhang J., Das Gupta S. and Gale C., *Phys. Rev. C* **50** (1994) 1617.

[32] Schuck P., private communication.

[33] Demoulins M., *et al.*, *Phys. Lett. B* **241** (1990) 479.

[34] Gutbrod H.H., Poskanzer A.M. and Ritter H.G., *Rep. Prog. Phys.* **52** (1989) 1267.

[35] Gossiaux P.-B. and Aichelin J., to be published.

[36] Cugnon J., La Physique avec Mimas, CEA, Saclay (1987) p. 412.

[37] Bertsch G. and Cugnon J., *Phys. Rev. C* **24** (1981) 2514.

[38] Siemens P. and Rasmussen J., *Phys. Rev. Lett.* **42** (1979) 880.

[39] Stöcker H., *et al.*, *Nucl. Phys. A* **400** (1983) 63c.

[40] Stöcker H., *Nucl. Phys. A* **418** (1984) 587c.

[41] Röpke G., Schmidt M., Munchow L. and Schultz H., *Nucl. Phys. A* **399** (1983) 587.
[42] Baldo M., Lombardo U. and Schuck P., *Phys. Rev. C* **52** (1995) 975.
[43] Poggi G., *et al.*, *Nucl. Phys. A* **586** (1995) 755.
[44] Borderie B., *et al.*, preprint IPN Orsay, 1996, IPNO-DRE-96-11.
[45] Kuhn C., Ph.D. thesis, CRN Strasbourg, 1993.
[46] Nifenecker H. and Pinston J.A., *Ann. Rev. Nucl. Sci.* **40** (1990) 113.
[47] L'Hôte D., in Nuclear Matter and Hevay Ion Collisions, M. Soyeur, *et al.*, Eds. (Plenum Press, New York, 1989) p. 323
[48] Cugnon J., Mizutani T. and Vandermeulen J., *Nucl. Phys. A* **352** (1981) 505.
[49] Hagedorn R., Montvay I. and Rafelski J., Hadronic Matter at Extreme Energy Density, N. Cabibbo, Ed. (Plenum Press, New York, 1980) p. 49.
[50] Serot B.D. and Walecka J.D., in Advances in Nuclear Physics, vol. 16, J.W. Negele and E. Vogt, Eds. (Plenum Press, New York, 1986).
[51] Glendenning N.K., *Z. Phys. A* **326** (1987) 57.
[52] Glendenning N.K., *Z. Phys. A* **327** (1987) 295.
[53] Nambu Y. and Jona-Lasinio G., *Phys. Rev.* **122** (1961) 345.
[54] Jaminon M. and Van den Bossche B., *Nucl. Phys. A* **582** (1995) 517.
[55] Ko C.M., Li Q. and Wang R., *Phys. Rev. Lett.* **59** (1987) 1084.
[56] Blättel B., *et al.*, *Phys. Rev. C* **38** (1988) 1767.
[57] Botermans W. and Malfliet R., *Phys. Lett. B* **215** (1988) 617.
[58] Botermans W. and Malfliet R., *Phys. Rep. C* **198** (1990) 115.
[59] Schönhofen M., Ph.D. Thesis, GSI report GSI-90-16.
[60] Siemens P.J., Soyeur M., White G.D., Lantto L.J. and Davies K.T.R., *Phys. Rev. C* **40** (1989) 2641.
[61] Mrowczynski S. and Heinz U., *Ann. Phys.* **229** (1994) 1.
[62] Welke G., private communication.
[63] ter Haar B. and Malfliet R., *Phys. Rev. C* **36** (1987) 1611.
[64] Metag V., *Nucl. Phys. A* **553** (1993) 283c.
[65] Schröter A., *et al.*, *Nucl. Phys. A* **553** (1993) 775c.
[66] Wolf Gy., Cassing W. and Mosel U., cited in [64].
[67] Pang Y., Schlagel T.J. and Kahana S.H., *Phys. Rev. Lett.* **68** (1992) 1743.
[68] Giacomelli G., *Int. J. Mod. Phys. A* **5** (1990) 223.
[69] Brenner A.E., *et al.*, *Phys. Rev. D* **26** (1982) 1497.
[70] Antreasyan D., *et al.*, *Phys. Rev. Lett.* **38** (1977) 112.
[71] Schwinger J., *Phys. Rev.* **82** (1951) 664.
[72] Wong C.Y., Introduction to High-Energy Heavy Ion Collisions (World Scientific Press, Singapore, 1994).
[73] Veneziano G., *Il Nuovo Cimento A* **57** (1968) 190.
[74] Nambu Y., in Symmetry and Quark Model, R. Chand, Ed. (Gordon & Breach, New York, 1970).
[75] Susskind L., *Il Nuovo Cimento A* **61** (1970) 457.
[76] Regge T., *Il Nuovo Cimento* **14** (1959) 951.
[77] Andersson B., Gustafson G. and Söderberg B., *Z. Phys. C* **20** (1983) 317.
[78] Artru X. and Mennessier G., *Nucl. Phys. B* **70** (1974) 93.

[79] Muta T., Foundations of Quantum Chromodynamics (World Scientific Press, Singapore, 1987).

[80] Christ N.H., *Nucl. Phys. A* **544** (1992) 81c.

[81] Cugnon J., Jaminon M. and Van den Bossche B., *Nucl. Phys. A* **598** (1996) 515.

[82] Sailer K., Müller B. and Greiner W., UFTP preprint 217/1988.

[83] Barton A., *et al.*, *Phys. Rev. D* **27** (1983) 2580.

[84] WA80 Collaboration, Sorensen S., *et al.*, *Z. Phys. C* **38** (1988) 3.

[85] NA36 Collaboration, Greiner D.E., *et al.*, *Nucl. Phys. A* **544** (1992) 309c.

[86] Braun-Munzinger P., *et al.* (E814 Collaboration), *Nucl. Phys. A* **544** (1992) 137c.

[87] Elze Th., preprint Univ. Heidelberg, 1990.

[88] Blaizot J.-P., Ollitrault J.Y. and Iancu E., Saclay preprint T95/087, 1995.

[89] Bjorken J.D., *Phys. Rev. D* **27** (1983) 140.

[90] Werner K. and Koch P., *Z. Phys. C* **47** (1990) 255.

[91] Werner K., *Phys. Rep.* **232** (1993) 87.

[92] Capella A., *et al.*, *Z. Phys. C* **33** (1987) 541.

[93] Möhring H.J., *et al.*, *Nucl. Phys. A* **525** (1991) 493c.

[94] Kaidalov A., *Nucl. Phys. A* **525** (1991) 39c.

[95] Gyulassy M., preprint CERN-TH 4794/87.

[96] Sjöstrand T. and van Zijl M., *Phys. Rev. D* **36** (1987) 2019.

[97] Wang X.N. and Gyulassy M., *Phys. Rev. D* **44** (1991) 3501.

[98] Sörge H., Stöcker H. and Greiner W., *Nucl. Phys. A* **498** (1989) 567c.

[99] Zymanyi J., Budapest Heavy Ions Meeting, J. Nemeth, Ed. (1994) to appear.

[100] Marchesini G. and Webber B.R., *Nucl. Phys. B* **238** (1984) 1.

[101] Geiger K. and Müller B., *Nucl. Phys. B* **369** (1992) 600.

[102] Gyulassy M., *Nucl. Phys. A* **590** (1995) 431c.

[103] Ruuskanen P.V., *Nucl. Phys. A* **522** (1991) 255c.

[104] Ruuskanen P.V., *Nucl. Phys. A* **544** (1992) 169c.

[105] Baglin C., *et al.*, *Phys. Lett. B* **255** (1991) 459.

[106] Matsui T. and Satz H., *Phys. Lett. B* **178** (1986) 416.

[107] Baglin C., *et al.*, NA38 Collaboration, *Phys. Lett. B* **272** (1991) 449.

[108] Blaizot J.-P. and Ollitrault J.Y., *Phys. Lett. B* **217** (1989) 386.

[109] Cugnon J. and Gossiaux P.-B., *Z. Phys. C* **58** (1993) 95.

[110] Cugnon J. and Gossiaux P.-B., *Phys. Lett. B* **359** (1995) 375.

[111] Gossiaux P.-B., Ph.D. Thesis, University of Liège (1993).

[112] Gerschel C. and Hüfner J., *Nucl. Phys. A* **544** (1992) 513c.

[113] Aubert J.J., *et al.*, *Nucl. Phys. B* **213** (1983) 1.

[114] Gerschel C., Quark Matter Conference (Heidelberg, 1996).

[115] Braaten E. and Pisarski R.D., *Nucl. Phys. B* **339** (1990) 310.

[116] Weldon H.A., *Phys. Rev. D* **26** (1982) 2789.

[117] Nagamiya S., *Nucl. Phys. A* **544** (1992) 5c.

[118] Koch P., Müller B. and Rafelski J., *Phys. Rep. C* **142** (1986) 783.

[119] Rafelski J., *Nucl. Phys. A* **544** (1992) 279c.

[120] Abatzia S., *et al.*, WA85 Collaboration, *Nucl. Phys. A* **544** (1992) 321c.